The fungal peptide toxin candidalysin induces distinct membrane repair mechanisms compared to bacterial pore-forming toxins

Roshan Thapa[1,†], Victor Kayejo[1,‡], Bernhard Hube[2,3], Julian R. Naglik[3] and Peter A. Keyel[1,*]

[1]Department of Biological Sciences
Texas Tech University
Lubbock, TX 79409

[2]Department of Microbial Pathogenicity Mechanisms
Leibniz Institute for Natural Product Research and Infection Biology-Hans Knoell Institute (HKI)
Jena, Germany

[3]Institute of Microbiology, Friedrich Schiller University, Jena, Germany

[4]Centre for Host-Microbiome Interactions
Faculty of Dental, Oral & Craniofacial Sciences
King's College London
London, SE1 1UL, UK

*to whom correspondence should be addressed
Peter Keyel
Department of Biological Sciences
Biology Rm 108
Box 43131
Lubbock, TX 79409-3131
tel: (806) 834-6248
fax: (806) 742-2963
email: peter.keyel@ttu.edu

[†]current address:
Charles River Laboratories, Inc.
Mattawan, MI 49071

[‡]current address:
Biomedical Graduate Program
Texas A&M University
College Station, TX

Running Title: Chloride protects cells from candidalysin-mediated killing

Keywords: *Candida albicans*; candidalysin; pore-forming toxin; ion-flux; annexin; membrane repair

Abstract

The common fungal pathogen, *Candida albicans*, relies on the pore-forming toxin candidalysin to damage host cells. Cells resist other pore-forming toxins by Ca^{2+} dependent microvesicle shedding and annexins (cholesterol-dependent cytolysins, CDCs), or annexins and patch repair (aerolysin). However, it is unclear which Ca^{2+} dependent repair mechanism(s) resists candidalysin. Here, we determined the involvement of different Ca^{2+} dependent repair mechanisms to candidalysin and compared responses to CDCs and aerolysin using flow cytometry and high-resolution microscopy. We report that candidalysin triggered Ca^{2+}-dependent repair, but patch repair and ceramide failed to provide significant protection. MEK-dependent repair and annexins A1, A2 and A6 contributed partially to repairing damage caused by candidalysin. However, annexin translocation after candidalysin challenge was delayed compared to CDCs or aerolysin challenge. Surprisingly, extracellular Cl^- improved cell survival after candidalysin challenge, but not after challenge with a CDC or aerolysin. Finally, we found that candidalysin is removed via extracellular vesicle shedding. These findings reveal that Ca^{2+} dependent microvesicle shedding protects cells from candidalysin and can be engaged by multiple molecular mechanisms during membrane repair.

62 **Introduction**

63 One leading cause of mucosal and life-threatening systemic fungal infections is *Candida*
64 *albicans*[1]. The morphological transition of *C. albicans* from a yeast to a filamentous hyphal form
65 is crucial for host cell invasion[2]. Host cell damage after hyphal invasion is promoted by secretion
66 of a key virulence factor—the peptide toxin candidalysin[3]. The precursor peptide of candidalysin
67 is embedded in the polyprotein Extent of cell elongation 1 protein (Ece1p) [3]. Candidalysin is
68 released from Ece1 by Kex1p and Kex2p mediated proteolytic processing to produce Ece1-III_{62-}
69 $_{93}$[3-5]. Candidalysin can bind to glucosaminoglycans (GAGs) and other potential molecules and
70 form <8 nm lytic pores that cause epithelial damage and cell death[3,4,6-9]. While host damage by
71 bacterial toxins has been extensively studied, the mechanisms by which cells survive
72 candidalysin attack are less explored.

73

74 Several Ca^{2+}- dependent membrane repair mechanisms protect cells from damage. Pathways
75 that resist pore-forming toxins (PFTs) include the physical blockade of the pore (clogging),
76 autophagy, the hetero/homotypic fusion of internal vesicles (patch repair), and removal of the
77 toxin on microvesicles (microvesicle shedding) [10,11]. Mechanistically, a wide variety of proteins
78 and lipids enable these pathways to reseal damage. Clogging of pores occurs when annexins
79 form crystalline arrays on the membrane[12,13]. Autophagy can reseal damage by recruitment of
80 LC-3 and formation of the autophagosomal membrane[14]. Patch repair represents the fusion of
81 endosomes and lysosomes with the plasma membrane, which then reseals pores via vertex
82 fusion[11]. A wide range of proteins mediate patch repair, including the muscle protein dysferlin[11].
83 Toxin pores can be removed via sequestration and shedding on microvesicles[15-18]. Shedding
84 can be energy and protein-independent, but lipid-dependent[15,18], or activated by proteins.
85 Proteins that drive shedding during repair include the endosomal sorting complex required for
86 transport (ESCRT) [17] and mitogen activated protein kinase kinase (MEK) signaling, partially via
87 annexin A2[16]. Other annexins may also be shed on microvesicles[16,19]. However, different pore-

88 forming toxins trigger distinct subsets of these repair pathways[20]. Understanding which
89 mechanisms are triggered by candidalysin will help identify key pathways that promote repair.
90
91 Prior work with candidalysin investigating repair responses identified three repair pathways.
92 Repair against candidalysin is Ca^{2+}-dependent, and can involve ESCRT-III mediated blebbing,
93 lysosomal exocytosis and autophagy[3,14,21,22]. Candidalysin also triggers MEK signaling that
94 promotes epithelial cell survival at late time points[23]. However, the role of other Ca^{2+}- dependent
95 repair mechanisms in resisting candidalysin damage, and the relative importance of each
96 pathway, remains unknown.
97
98 A comparative analysis of PFTs is expected to reveal which pathways are best targeted to
99 improve cellular resistance to specific toxins. Our prior work compared two other PFTs:
100 streptolysin O (SLO) from *Streptococcus pyogenes* with aerolysin from *Aeromonas hydrophila*[20].
101 SLO and aerolysin belong to two distinct, well-studied PFT subfamilies, the cholesterol
102 dependent cytolysins (CDCs) and the aerolysin family, respectively[24]. These toxins are repaired
103 via distinct mechanisms[20]. About 70% of the Ca^{2+}-dependent repair for SLO uses MEK-
104 dependent microvesicle shedding, while annexins and ceramide elevation also promote
105 survival[16,20]. In contrast, Ca^{2+} overload kills aerolysin-challenged cells, while patch repair
106 promotes resistance to aerolysin[20]. Therefore, we selected SLO and aerolysin to compare the
107 relative importance of repair mechanisms to resist candidalysin.
108
109 Here, we compared the mechanisms of repair between candidalysin and two bacterial pore-
110 forming toxins that engage distinct repair mechanisms. We found that candidalysin was not
111 resisted via patch repair or ceramide elevation. We observed partial protection from MEK-
112 dependent repair and annexins A1, A2 and A6, though annexin translocation after candidalysin
113 challenge was delayed. Surprisingly, we found that elevating extracellular Cl^- improved cell

114 survival against candidalysin, which was not observed for SLO or aerolysin. Finally,
115 microvesicle shedding removed candidalysin from cells. Overall, these data suggest
116 candidalysin triggers a distinct subset of membrane repair mechanisms.

117 **Results**

118 **Candidalysin cytotoxicity against nucleated cells is intermediate between SLO and**
119 **aerolysin**

120 To compare repair mechanisms between candidalysin, SLO and aerolysin, we first normalized
121 toxin activity using hemolytic activity in human erythrocytes. We used hemolytic activity instead
122 of toxin mass because it normalizes toxin activity for better comparison, provides a measure of
123 cellular resistance mechanisms, is consistent with our prior work, and controls for variation in
124 the specific activity between toxin preparations[16,20]. We challenged HeLa cells with a range of
125 toxin doses, calculated the specific lysis due to toxin, fit the dose-response curves to a logistic
126 model, and calculated the toxin dose needed to kill 50% of the cells (LC_{50}) for each experiment[25]
127 (Fig 1). We first determined the minimum time range to best measure cell damage and repair for
128 each toxin to minimize non-specific lysis. We challenged HeLa cells with candidalysin, aerolysin
129 and SLO for 30 min, 1 h and 2 h and measured the cell viability by MTT and LDH assay
130 (Supplementary Figs S1, S2). Similar to aerolysin, cytolytic activity by candidalysin plateaued at
131 1 h, whereas SLO plateaued at 30 min (Supplementary Fig S1). Therefore, we used 1 h for
132 candidalysin and aerolysin and 30 min for SLO to compare repair mechanisms.

133

134 We next controlled for cytotoxicity due to any impurities in toxin purification by comparing wild
135 type toxins with an equivalent mass of toxins mutated to cripple cytolytic activity using flow
136 cytometry. None of the mutant toxins were cytotoxic to HeLa cells (Fig 1A-C), despite the
137 candidalysin mutant retaining 10% of wild type hemolytic activity (Supplementary Table S1). In
138 contrast, wild type candidalysin was less toxic than aerolysin, but more toxic than SLO (Fig 1).
139 The LC_{50} for candidalysin (73.7 ±4.65 HU/mL) was between aerolysin (32.6 ±7.08 HU/mL) and
140 SLO (426.1 ± 38.8 HU/mL) (Fig 1D). These data suggest that candidalysin triggers less repair
141 than SLO, but more than aerolysin.

142

143 **Candidalysin triggers Ca^{2+}-dependent repair**

144 Most membrane repair mechanisms described to date require Ca^{2+} influx. One key difference
145 between aerolysin and SLO is that Ca^{2+}-influx is toxic following aerolysin challenge, but
146 protective against SLO[20]. Previous results showed that Ca^{2+} influx is protective during
147 candidalysin challenge[3,21,22]. We confirmed the impact of Ca^{2+}-influx on cell survival following
148 candidalysin challenge by chelating extracellular Ca^{2+} with EGTA. Removing Ca^{2+} from the
149 extracellular medium sensitized HeLa cells to candidalysin, similar to what we observed for SLO
150 (Fig 1E, Supplementary Fig S3A). In contrast, removal of extracellular Ca^{2+} protected HeLa cells
151 from aerolysin (Fig 1E, Supplementary Fig S3A), consistent with previous results[20]. These data
152 suggest that candidalysin engages Ca^{2+} -dependent repair mechanisms, similar to those
153 triggered by SLO.

154

155 **Patch repair and ceramide fail to protect cells from candidalysin**

156 Our prior work[20] suggested that patch repair is a backup repair mechanism for SLO, while the
157 primary mechanism for aerolysin. Since candidalysin and SLO both trigger protective Ca^{2+}
158 influx, we hypothesized that patch repair would be a minor contributor to repair. To test this
159 hypothesis, we measured the ability of the well-characterized muscle patch repair protein
160 dysferlin[11,20] to promote survival against candidalysin. Dysferlin-deficient C2C12 myoblasts were
161 more sensitive than control C212 myoblasts to aerolysin and SLO (Fig. 2A; Supplementary Fig
162 S3B), consistent with prior results[20]. However, loss of dysferlin did not increase cellular
163 sensitivity to candidalysin (Fig. 2A; Supplementary Fig S3B). These data suggest that the patch
164 repair protein dysferlin does not contribute to repair triggered by candidalysin.

165

166 To confirm that patch repair is not significant for protection against candidalysin, we measured
167 the ability to dysferlin overexpression to protect non-muscle cells from cytotoxicity. Our prior
168 results showed that over-expression of dysferlin protects HeLa cells from both aerolysin and

169 SLO[20]. Consistent with prior results[20], we found that GFP-dysferlin transfection enhanced
170 cellular resistance against aerolysin and SLO compared to GFP-transfected cells(Fig 2B,
171 Supplementary Fig S3C). In contrast, GFP-dysferlin transfection failed to enhance cellular
172 resistance to candidalysin (Fig 2B, Supplementary Fig S3C). Based on these data, we conclude
173 that dysferlin-mediated patch repair fails to protect cells from candidalysin.
174
175 Since patch repair failed to protect cells against candidalysin, we next tested other mechanisms
176 of repair. Sphingolipids and ceramide contribute to protection against CDCs in multiple
177 systems[16,26-28]. We previously showed that ceramide accumulation by inhibiting UDP-glucose
178 ceramide glucosyltransferase protects cells from CDCs without perturbing sterol or
179 sphingomyelin levels[16]. We tested the hypothesis that ceramide accumulation also promotes
180 cellular resistance to candidalysin. While ceramide accumulation protected cells from SLO as
181 previously described[16], it did not alter cell sensitivity to either aerolysin or candidalysin (Fig 2C,
182 Supplementary Fig S3D). To confirm that we did not alter cellular levels of either sphingomyelin-
183 cholesterol complexes, nor total sphingomyelin, we measured them using wild-type ostreolysin
184 A (OlyA)–mCherry[29], or OlyA^{E69A}-mCherry[30], respectively. Ceramide accumulation did not alter
185 these lipids in the plasma membrane (Fig 2D). Based on these findings, we conclude ceramide
186 does not provide significant cellular protection against candidalysin.
187
188 **Chloride ions protect cells from candidalysin**
189 We next tested the contribution of K^+ efflux to candidalysin resistance, because prior results[31]
190 suggested it contributes to resisting pore-forming toxins. We blocked K^+ efflux by adding 150
191 mM KCl to the culture medium. While blocking K^+ efflux did not impact cell survival following
192 SLO or aerolysin challenge, blocking K^+ efflux protected HeLa cells from candidalysin (Fig 3A,
193 Supplementary Fig S4A). We next determined the impact of extracellular KCl in a second cell
194 type, primary bone marrow-derived macrophages (BMDM). We used caspase1/11$^{-/-}$ BMDMs to

195 rule out toxin-induced pyroptosis[32]. KCl protected BMDM from both candidalysin and aerolysin,
196 but sensitized cells to SLO (Fig 3B, Supplementary Fig S4B). To determine whether Ca^{2+} influx
197 or K^+ efflux were more important, we blocked both, and measured cell viability after toxin
198 challenge. The presence of KCl overcame the EGTA-induced sensitivity to candidalysin in
199 BMDM (Fig 3B, Supplementary Fig S4B). Based on these results, extracellular KCl protects
200 cells against candidalysin.
201
202 We next tested the ability of enforced K^+ flux to increase cell death in response to candidalysin.
203 We treated HeLa cells with potassium/proton ionophore nigericin, or EGTA, with and without
204 150 mM KCl prior to candidalysin challenge. Nigericin does not interfere with candidalysin
205 activity[22]. Nigericin sensitized cells to candidalysin (Fig 3C, Supplementary Fig S4C). However,
206 nigericin also overcame the inhibition provided by KCl, suggesting that its proton ionophore
207 capabilities contribute to sensitizing cells to candidalysin (Fig 3C, Supplementary Fig S4C). In
208 contrast, KCl overcame the ability of Ca^{2+}-chelation to sensitize cells to candidalysin. We
209 interpret these results to suggest that ion flux plays an important role in cell death due to
210 candidalysin.
211
212 To distinguish between the contribution of the K^+ and Cl^- ions, we compared the ability of
213 multiple salts to protect cells against toxins. We first challenged HeLa cells with toxin in the
214 presence or absence of 150 mM KCl or NaCl. While neither salt protected cells from aerolysin
215 or SLO, both salts afforded cells similar protection against candidalysin (Fig 3D, Supplementary
216 Fig S4D). We next tested 300 mM dextrose to control for osmolarity, and several potassium and
217 chloride salts at 150 mM. Cell sensitivity to SLO was unaffected by all salts tested (Fig 3E,
218 Supplementary Fig S4E). Cell sensitivity to aerolysin trended down upon dextrose treatment,
219 but increased with NH_4Cl (Fig 3E, Supplementary Fig S4E). In contrast, cells were protected
220 against candidalysin in the presence of KCl or NH_4Cl, but not potassium acetate (Fig 3E,

221 Supplementary Fig S4E). We interpret these data to indicate that extracellular chloride may
222 protect cells from candidalysin, but not aerolysin or SLO.
223
224 **Candidalysin triggers MEK dependent repair**
225 We next tested the role of MEK signaling in candidalysin resistance. MEK is activated by
226 candidalysin, and signaling via ERK is important for cell survival at late time points[22], so it is
227 possible that the ERK-independent signaling protects cells at early time points like it does for
228 CDCs[16]. We blocked MEK activation with the MEK inhibitor U0126 (Fig 4A), which is specific for
229 MEK in this system[16]. MEK inhibition increased the sensitivity of HeLa cells to both candidalysin
230 and SLO, but not to aerolysin (Fig 4B-D, Supplementary Fig S5). When compared to the total
231 Ca^{2+}-dependent repair, MEK inhibition accounted for ~40% of Ca^{2+}-dependent repair against
232 candidalysin and ~50% of Ca^{2+}-dependent repair against SLO. Overall, candidalysin triggers
233 MEK-dependent repair, though to a lesser extent than CDCs.
234
235 **Annexins provide limited and delayed protection against candidalysin**
236 We further explored the repair pathway downstream of MEK activation. One downstream target
237 of MEK-dependent repair is Annexin A2 (A2) [16]. Annexins A1 and A6 are independent of MEK
238 activation, but are involved in membrane repair[13,16,33]. We tested the role of these three
239 annexins in the repair of candidalysin-mediated damage using siRNA. Annexin knockdown
240 efficiency ranged from 60% for A6 to 85% for A2 (Fig. 5A-B). Knockdown of each annexin
241 sensitized cells to candidalysin, aerolysin and SLO (Fig 5C, Supplementary Fig S6). These
242 results suggest that annexins promote cellular resistance to candidalysin.
243
244 We further explored the contribution of annexins to repair against candidalysin using high-
245 resolution live cell imaging. A2 translocates rapidly to the plasma membrane[19], except when
246 MEK is inhibited[16]. Annexin membrane recruitment is faster for CDCs compared to aerolysin[20].

247 We challenged A2-GFP or A6-YFP transfected cells with candidalysin, mutant candidalysin as a
248 control, aerolysin or SLO, and imaged annexin dynamics (Fig 5D-I, Supplementary Fig S7A, B,
249 Videos 1 & 2). Annexins translocated to the membrane in ~20% of A2-GFP+ cells and ~60%
250 A6-YFP+ cells after candidalysin challenge, compared to translocation in 75-90% of cells
251 challenged with aerolysin or SLO challenge (Fig 5D, G). To measure cell viability during annexin
252 translocation, we analyzed TO-PRO3 uptake. Annexins translocated to the membrane without
253 TO-PRO3 accumulation (Supplementary Fig S7C, Videos 1 & 2).We measured annexin
254 translocation by determining the half time ($t_{1/2}$) of depletion of the annexin from the cytosol, plus
255 the half time ($t_{1/2}$) of annexin enrichment on the plasma membrane. Similar to previous
256 results[16,20], the $t_{1/2}$ for A2 and A6 depletion and recruitment was ~7 min and ~8 min,
257 respectively, for SLO, and ~12 min for aerolysin (Fig 5E, F, H, I, Supplementary Fig S7A, B,
258 Videos 1 & 2). In contrast, active candidalysin triggered delayed cytosolic depletion and
259 membrane recruitment of both A2 and A6, with a $t_{1/2}$ of ~40 min cytoplasmic annexin depletion
260 and membrane recruitment of A2 (Fig 5E, F, H, I, Supplementary Fig S7A, B, Videos 1 & 2).
261 Surprisingly, A6 was recruited to the membrane faster ($t_{1/2}$ ~25 min) than A2 during candidalysin
262 challenge (Fig 5E, F, H, I, Supplementary Fig S7A, B, Videos 1 & 2). This is similar to the
263 situation when MEK is not active in repair[16]. Taken together, we interpret these data to suggest
264 that annexins contribute to candidalysin resistance, but they are recruited later in the repair
265 process than for other toxins.
266

267 **Microvesicle shedding removes candidalysin from cells**

268 Since annexin clogging and patch repair had minimal to no impact on repair, we tested the
269 hypothesis that candidalysin is shed on microvesicles. We challenged cells with a sublytic dose
270 of each toxin, or the defective candidalysin mutant to control for spontaneous vesicle release.
271 All three active toxins were shed on microvesicles, though oligomeric aerolysin also remained
272 present on the cell surface (Fig 6). Along with the active toxins, A2 and A6 were shed in

273 microvesicles for all three toxins (Fig 6), consistent with the previous results[18,20]. Neither A1 nor
274 the Endosomal Sorting Complex Required for Transport (ESCRT) protein ALG-2-interacting
275 protein X (ALIX) were shed following candidalysin challenge, though they were shed in
276 response to aerolysin (Fig 6). To distinguish between shed vesicles and cellular debris from
277 lysed cells, we probed for the nuclear proteins Lamin A/C. Lamin A/C was not shed from cells
278 challenged with active toxins (Fig. 6), indicating that the microvesicle fraction did not contain
279 detectable cellular debris. Thus, candidalysin is shed on microvesicles by cells.

280 **Discussion**

281 In this study, we determined which repair mechanisms respond to candidalysin and compared
282 these responses to pore-forming toxins from the CDC and aerolysin families. We found that
283 candidalysin triggered a distinct repair profile compared to both CDCs and aerolysin. Similar to
284 CDCs, candidalysin triggered Ca^{2+}-dependent repair and microvesicle shedding. However,
285 candidalysin triggered less MEK-dependent repair than CDCs. In contrast to both aerolysin and
286 CDCs, extracellular chloride, but not patch repair, protected cells from candidalysin. Finally,
287 annexin recruitment was reduced and delayed compared to other toxins. Based on our data, we
288 conclude that candidalysin triggers distinct molecular mechanisms to drive microvesicle
289 shedding, which suggests approaches to bolster specific membrane repair mechanisms could
290 reduce *Candida* pathogenicity.

291

292 Our present work integrates and expands the repair mechanisms used to resist candidalysin.
293 Our results are consistent with prior work[3,21,22] showing the Ca^{2+}-dependence of repair resisting
294 candidalysin. We find additional active repair mechanisms that resist candidalysin beyond
295 ESCRT-III mediated shedding[21] and autophagy[14], including a chloride trigger, and involvement
296 of MEK and annexins. Since MEK inhibition had partial effect on repair, and annexin
297 translocation was delayed, shedding via ESCRT activation and via MEK might represent two
298 distinct repair pathways that both trigger microvesicle shedding. Interestingly, prior work
299 observed Alix and Galectin-3 recruitment to roughly half of the sites of *Candida albicans*
300 penetration[14], suggesting that the other sites were either undamaged, or that different repair
301 pathways were engaged. Where ESCRT pathways diverge from other repair pathways
302 downstream of Ca^{2+}-influx remains to be determined.

303

304 Our findings here differ from others' results in the role of lysosomal exocytosis and/or patch
305 repair to resist candidalysin. Prior work observed recruitment of lysosomal proteins to the site of

306 damage[14,21], while our dysferlin assay showed no contribution of dysferlin to protection. Since
307 the prior work used *Candida albicans* for damage instead of candidalysin alone, another protein
308 or factor could trigger patch repair in those systems. Another possibility is that dysferlin
309 recruitment/involvement fails to capture the full spectrum of patch repair, so assay-specific
310 differences could account for the different results. Finally, it is possible that lysosomal
311 exocytosis contributes to the cellular return to homeostasis, instead of directly contributing to
312 repair of candidalysin-induced lesions. Our assay is focused on repair because it measures cell
313 viability instead of protein relocalization, so it would not capture post-repair membrane
314 rearrangements. In summary, our findings provide a novel perspective to cellular repair
315 responses to candidalysin
316
317 One key novel finding was that increasing the extracellular Cl^- concentration protected cells from
318 candidalysin, in contrast to any role of Cl^- for SLO or aerolysin. Several lines of evidence
319 support Cl^- as the active ion over K^+ or changes in osmolarity, despite the role of K^+ channels in
320 cell death[34]. First, prior work using glibenclamide to block K^+ channels did not impact damage
321 due to candidalysin[35]. Second, addition of dextrose or potassium acetate failed to enhance
322 cellular resistance to candidalysin. Third, nigericin-mediated death in our assays was not
323 blocked by extracellular K^+. Finally, multiple Cl^- salts provided protection, while salts without Cl^-
324 and dextrose all failed to protect cells. While it remains possible that monovalent cations
325 collectively provide protection, we note that the electrochemical gradients driven by Na^+ and K^+
326 run in opposite directions[34], yet both NaCl and KCl provided similar protection. In contrast, the
327 typical extracellular Cl^- concentration is ~2-3 fold higher than intracellular concentrations[36]. How
328 increasing extracellular Cl^- improves cellular resistance remains to be determined.
329
330 There are some potential mechanisms by which Cl^- could enhance resistance to candidalysin.
331 Chemically, Cl^- could interact with the positively charged candidalysin, and prevent cellular

332 binding and/or oligomerization. Chloride salts like ammonium chloride can promote autophagy[37].
333 Given the role for autophagy in repairing candidalysin lesions[14], it is possible that extra Cl^-
334 enhances autophagy, which drives repair. Alternatively, chloride channels could promote repair.
335 Proteins in the anoctamin family (TMEM16A-F) include Ca^{2+}-dependent Cl^- channels[38-40]. For
336 example, Anoctamin 6/TMEM16F contributes to the outwardly rectifying chloride channel and is
337 involved in cell death and size[40]. Anoctamin 6 is previously implicated in promoting repair
338 against both LLO and SLO[39]. The counterargument is that we observed an effect for Cl^- against
339 candidalysin, but not SLO. Thus, the mechanism by which increased extracellular Cl^- enhances
340 repair against candidalysin is a future avenue for research.
341
342 Another novel finding was that annexins had a delayed response to candidalysin compared to
343 SLO or aerolysin. Taken with our findings that loss of either A1, A2 or A6 contributed mild
344 effects to reducing repair, we propose that annexins serve as a backup mechanism to resist
345 candidalysin. In many cases, A6 translocated faster than A2, which further suggests that MEK
346 dependent repair is not the primary means of resisting candidalysin. Alternatively, candidalysin
347 could trigger a programmed cell death pathway, and annexin translocation is either dampened
348 by the death pathway, or activation delayed until just prior to cell lysis. Future directions include
349 determining the interplay between programmed cell death pathways and membrane repair.
350
351 Our work had several limitations due to the experimental system. We did not test candidalysin in
352 the context of the whole pathogen. While we used primary macrophages for some experiments,
353 we used HeLa cells for many experiments, which could differ from the epithelial cells invaded by
354 *C. albicans*. We relied on prior work[14,21] for the contribution of autophagy and ESCRT to repair
355 against candidalysin. While we found an effect from Cl^- to enhance repair, the signaling
356 intermediates between Cl^- and repair remain a future research direction. Similarly, the toxin
357 determinants that determine which repair pathways are activated remains unknown.

358

359 In summary, we compared repair responses between candidalysin and toxins from two other
360 families, CDCs and aerolysins. Candidalysin triggered a distinct repair profile compared to these
361 toxins that included Ca^{2+}-dependent repair, microvesicle shedding and resistance in the
362 presence of elevated chloride levels. In contrast to other toxins, annexin recruitment was
363 reduced and delayed, dysferlin-mediated patch repair did not contribute to repair, and MEK-
364 dependent repair was reduced. Overall, we conclude that candidalysin triggers distinct
365 membrane repair mechanisms that could be enhanced to reduce *C. albicans* pathogenicity.

366 **Materials and Methods**

367 ***Reagents*.** All reagents were from Thermo Fisher Scientific (Waltham, MA, USA) unless
368 otherwise noted. The MEK1/2 inhibitor U0126 was from Tocris (Minneapolis, MN, USA) (Cat#
369 1144) or Alfa Aesar (Cat# J61246). Negative control siRNA or Silencer pre-designed siRNAs for
370 annexin A1 (Assay ID: 146988), A2 (Assay ID: 147285) or A6 (Assay ID: 241008) were from
371 Invitrogen (Waltham, MA, USA). Propidium iodide (PI) was from Biotium (Fremont, CA, USA)
372 (Cat # 40016). MTT reagent (Cat# 2809-1G) was from BioVision (Milpitas, CA, USA). D-threo-1-
373 phenyl-2-hexadecanoylamino-3-morpholino-1-propanol ·HCl (PPMP) was from Avanti Polar
374 Lipids (Alabaster, AL, USA) (catalog no. 870792).

375 **Antibodies.** The anti-annexin A1 monoclonal antibody (mAb) clone CPTC-ANXA1-3-s was
376 deposited to the Developmental Studies Hybridoma Bank (DSHB) by Clinical Proteomics
377 Technologies for Cancer (DSHB Hybridoma Product CPTC-ANXA1-3) and anti-Lamin A/C mAb
378 clone MANLAC-4A7-s was deposited to the DSHB by GE Morris (DSHB Hybridoma Product
379 MANLAC1(4A7)). Both were obtained from the DSHB, created by the NICHD of the NIH and
380 maintained at the University of Iowa, Department of Biology (Iowa City, IA, USA). Anti-β-actin
381 mAb clone AC-15 (Cat# GTX26276) was from GeneTex (Irvine, CA, USA). Anti-SLO mAb clone
382 6D11 (catalog: NBP1-05126) was from Novus Biologicals (Littleton, CO, USA). Anti-Alix mAb
383 clone 3A9 mAb was from BioLegend (San Diego, CA, USA). The anti-aerolysin rabbit polyclonal
384 antibody[20] and myc-tagged CAL1-H1 anti-candidalysin camelid nanobody[41] were previously
385 described. Anti-MEK (Cat# 9122L), anti-phospho-MEK [Ser217/Ser221] (Cat# 9121S), anti-ERK
386 p44/42 (Cat# 9102S), and anti-phospho-ERK [Thr202/Tyr404] (Cat# 9101S) rabbit polyclonal
387 antibodies were from Cell Signaling Technologies (Danvers, MA, USA). Anti-mouse-IgG (Cat#
388 711-035-151), anti-rabbit-IgG (Cat# 711-035-152), or anti-alpaca IgG (Cat# 128-035-230)
389 conjugated to horse radish peroxidase (HRP) were from Jackson ImmunoResearch (West
390 Grove, PA, USA).

391 ***Plasmids.*** The pET22b plasmids encoding His-tagged aerolysin and aerolysin^{Y221G} were kind
392 gifts from Gisou van der Goot (École Polytechnique Fédérale de Lausanne, Canton of Vaud,
393 Switzerland)[42]. The wild type aerolysin contains Q254E, R260A, R449A and E450Q mutations
394 and the C-terminal KSASA was replaced with NVSLSVTPAANQLE HHHHHH compared to
395 sequences in GenBank (i.e. M16495.1). Human annexin A6 fused to YFP was a generous gift
396 from Annette Draeger (University of Bern, Bern, Switzerland)[43]. Human annexin A2-GFP
397 (Addgene plasmid no. 107196) was from Addgene[44]. OlyA fused to mCherry in pET21c(+) was
398 a kind gift from Kristina Sepčić (University of Ljubljana, Ljubljana, Slovenia)[45], and the E69A
399 mutation was introduced as described[16]. Cysteine-less, His-tagged wild type and G398V/G399V
400 monomer-locked (ML) SLO codon-optimized for *Escherichia coli* expression[16] and GFP-
401 dysferlin[20] were previously described.

402 ***Mice.*** All experimental mice were housed and maintained according to Texas Tech University
403 Institutional Animal Care and Use Committee (TTU IACUC) standards, adhering to the Guide for
404 the Care and Use of Laboratory Animals (8th edition, NRC 2011). The TTU IACUC approved
405 mouse use. Casp1/11$^{-/-}$ mice on the C57BL/6 background were purchased from the Jackson
406 Laboratory (Bar Harbor, ME, USA) (stock #016621). Mice of both sexes aged 6–15 weeks were
407 used to prepare bone-marrow derived macrophages (BMDM). Sample size was determined as
408 the minimum number of mice needed to provide enough bone marrow for experiments.
409 Consequently, no randomization or blinding was needed. Mice were euthanized by asphyxiation
410 through the controlled flow of pure CO_2 followed by cervical dislocation.

411 ***Cell culture.*** All cell lines were maintained at 37°C, 5% CO_2. HeLa cells (ATCC (Manassas, VA,
412 USA) CCL-2) were cultured in DMEM (Corning, Corning, NY, USA) supplemented with 10%
413 Equafetal serum blend (Atlas Biologicals, Fort Collins, CO, USA) and 1x L-glutamine (D10
414 medium). Casp1/11$^{-/-}$ BMDM were isolated from bone marrow and differentiated for 7-21 days in

415 DMEM supplemented with 30% L929 cell supernatants, 20% fetal calf serum (VWR Seradigm,
416 Radnor, PA, USA), 1 mM sodium pyruvate and 1x L-glutamine, as previously described[16,18].

417 ***Toxins.*** Wild-type (SIIGIIMGILGNIPQVIQIIMSIVKAFKGNK) and mutant
418 (SIIGIIMGILGNIPQVIQIIMSIVKAF**A**GN**A**) candidalysin were synthesized by Peptide Protein
419 Research, Ltd (Hampshire, UK) as previously described[3]. SLO, OlyA-mCherry, and pro-
420 aerolysin were induced in *E. coli* BL21 GOLD cells and purified as previously described[16,20,46].
421 Briefly, log phase cells were induced with 0.2% arabinose (SLO, SLO ML), or 0.2 mM IPTG
422 (OlyA-mCherry, OlyA^{E69A}-mCherry, pro-aerolysin, and pro-aerolysin^{Y221G}) for 3 h at room
423 temperature, frozen, lysed, and then purified using Nickel-NTA resin. Protein concentration was
424 determined by Bradford Assay (Supplementary Table S1). Purity was assessed by SDS-PAGE.
425 The hemolytic activity of each toxin was determined as previously described[16,20] using human
426 red blood cells (Zen-Bio, Research Triangle Park, NC, USA) (Supplementary Table S1). One
427 hemolytic unit (HU) is defined as the quantity of toxin required to lyse 50% of a 2% human red
428 blood cell solution in 30 min at 37°C in 2 mM $CaCl_2$, 10 mM HEPES, pH 7.4 and 0.3% BSA in
429 PBS[16,20,46]. We used HU/mL to normalize toxin activities across experiments and to achieve
430 consistent cytotoxicity across toxin preparations. Sublytic doses were defined as the highest
431 toxin concentration that killed <20% of target cells. For HeLa cells, the sublytic dose was 250
432 HU/mL for SLO, 62 HU/mL for aerolysin and 50 HU/mL for candidalysin. Pro-aerolysin was
433 activated using trypsin as previously described[20] prior to assays.

434 ***Transfection.*** HeLa cells were plated at 2×10^5 cells per 35 mm glass-bottom dish or per well
435 in a 6 well plate and transfected with 750 ng Annexin A6, Annexin A2, peGFP-N1 or GFP-
436 Dysferlin using Lipofectamine 2000 in Opti-MEM two days before imaging or cytotoxicity assays.
437 D10 media was replaced on the day after transfection. Transfection efficiencies for each
438 construct ranged between 65-80%. For RNAi, HeLa cells were plated at 2×10^5 cells in 6-well

439 plates and transfected the following day with 10 nM siRNA using Lipofectamine 2000 in Opti-
440 MEM for 48-72 h as previously described[16,20].

441 ***MTT/LDH Assays***. The MTT [3-(4,5-dimethylthiazol-2-yl)-2,5-diphenyltetrazolium bromide] and
442 LDH (lactate dehydrogenase) assays were performed and analyzed as previously described[20].
443 Briefly, HeLa cells were harvested and resuspended at 1×10^5 cells per well in a 96 well flat
444 bottom plate in DMEM (without Phenol Red) supplemented with 2 mM $CaCl_2$. Toxins were
445 diluted in DMEM according to hemolytic activity (wild-type toxins) or equivalent mass (mutant
446 non-hemolytic toxins), serially diluted two-fold, added to wells containing cells, and incubated for
447 30 min, 1 h or 2 h at 37°C. Triton-X-100 was added to a final concentration of 0.5% to four wells
448 containing cells as a positive control for maximum LDH release and incubated for 30 min. After
449 incubation, cells were centrifuged at 1200× g for 5 min at 4°C to pellet cells. Cell pellets were
450 assayed for MTT activity, while supernatants were assayed for LDH activity. For the MTT assay,
451 cells were resuspended in 1.1 mM MTT assay reagent in DMEM without Phenol Red and
452 incubated at 37°C for 4 h. Formazan was dissolved in SDS-HCl at 37°C overnight. A_{570} was
453 measured with a plate reader (Bio-Tek, Winooski, VT, USA). The % viable cells was calculated
454 as follows: % Viable = (Sample − Background)/(Control − Background) × 100. Then, % Specific
455 Lysis was calculated as 100% − Viable. For the LDH assay, cell supernatants were assayed per
456 the manufacturer's instructions. % LDH release was calculated as (Sample − Background)/
457 (Maximum LDH release − Background) × 100.

458 ***Flow Cytometry Assay.*** Cytotoxicity was performed as described[16,20,46]. Briefly, cells were
459 transfected for 48-72 h or incubated with 40 μM PPMP for 72 h to promote ceramide
460 accumulation[47]. $1x10^5$ cells were challenged in suspension with various toxin concentrations for
461 30 or 60 min at 37°C in RPMI supplemented with 2 mM $CaCl_2$ and 20 μg/mL PI. Cells were
462 analyzed on a 4-laser Attune Nxt flow cytometer. Assay variations included changes to the
463 media (replacing 2 mM $CaCl_2$ with 2 mM EGTA, adding 150 mM KCl, 150 mM NaCl, 300 mM

464 Dextrose, 150 mM potassium acetate, 150 mM NH_4Cl, or 20 μM nigericin), or serum-starving
465 cells in DMEM for 30 min at 37° C and pretreating with DMSO or 20 μM U0126 in serum-free
466 media for 30 min at 37° C. For analysis of cell lysis, we gated out the debris and then quantified
467 the percentage of cells with high PI fluorescence (2–3 log shift) (PI high), or background
468 fluorescence (PI negative). We calculated specific lysis as: % Specific Lysis = (% PI
469 $High^{Experimental}$ − % PI $High^{Control}$)/ (100 − % PI $High^{Control}$) × 100. The toxin dose needed to kill
470 50% of cells was defined as the Lethal Concentration 50% (LC_{50}) and was determined by
471 logistic modeling using Excel (Microsoft, Redmond, WA, USA) as previously described[25].

472 ***Fluorescent annexin shedding assays.*** Annexin translocation assays were performed as
473 previously described[16,20]. Briefly, HeLa cells were plated at 2×10^5 cells per 35 mm glass-
474 bottom dish and transfected with 750 ng A6-YFP or A2-GFP using Lipofectamine 2000 two days
475 prior to imaging. The transfection efficiency was ~65-80%. Transfected cells were challenged
476 with a sublytic toxin dose for active toxins (250 HU/mL SLO, 62.5 HU/mL aerolysin or 50 HU/mL
477 candidalysin) or mass equivalent of mutant candidalysin ($candidalysin^{mutAA}$) and imaged at 37°C
478 in RPMI, 25 mM HEPES pH 7.4, and 2 mM $CaCl_2$ with 2 μg/mL TO-PRO3 for 45 min using a
479 Fluoview 3000 confocal microscope (Olympus, Tokyo, Japan) equipped with a 60×, 1.42 NA oil
480 immersion objective and recorded using the resonant scanner at 1–3 s per frame. A6-YFP and
481 A2-GFP were excited using a 488 nm laser, while TO-PRO3 was excited with a 640 nm laser.
482 After 45 min, the assay was terminated by adding an equal volume of 2% Triton-X-100 to give a
483 final concentration of 1%. The percentage of cells showing fluorescent annexin translocation
484 was determined by comparing the intensity at 15 min to the intensity 1 min after toxin addition. If
485 these values were below 80% of the initial value, cells were considered to show annexin
486 translocation. In cells showing fluorescent annexin translocation, the extent of fluorescent
487 annexin depletion from cells was assessed by measuring the intensity from the middle of the
488 cell over time by plotting Z profiles in FIJI (NIH, Bethesda, MD, USA). Membrane accumulation

489 of annexins (A2 or A6) over time was calculated by determining the changes in the fluorescence
490 intensity along the edges of the cells of translocated cells by plotting the Z profile in FIJI. The
491 intensity was then normalized on a per-cell basis and individually analyzed cells were plotted.
492 TO-PRO3 uptake was determined in fluorescent annexin translocated cells by plotting the Z
493 profile of a nuclear subsample over time. The data were normalized to the integrated intensity of
494 the brightest point. The $t_{1/2}$ for annexin cytosolic depletion, membrane accumulation, or TO-
495 PRO3 uptake was calculated by measuring the half-maximal intensity between the starting
496 intensity and the average intensity of the last 4 min prior to Triton-X-100 addition. From the
497 multi-plane images, >25 cells were analyzed from at least three independent experiments and
498 graphed using Microsoft Excel. Quantified values for individual cells were represented with
499 Prism 10.4.1 (GraphPad, San Diego, CA, USA).

500 ***Bleach correction and supplemental videos.*** Images were exported as .tif and split into
501 individual monochromatic red, green, and blue channels in FIJI. For display (but not analysis),
502 bleach correction was performed as previously described[16] on the "green" channel cells by
503 histogram matching using FIJI followed by a median pass filter. The monochromatic images
504 were then merged to form RGB .tif files, time-stamped, annotated, and exported as AVIs for
505 supplementary videos.

506 **SDS-PAGE and immunoblotting.** Cells or proteins were dissolved in 95° C 1x SDS-sample
507 buffer, heated for 5 min at 95° C and sonicated. Samples were resolved on 10% polyacrylamide
508 gels at 170 V for ~90 min and transferred to nitrocellulose in an ice bath with transfer buffer
509 (15.6 mM Tris and 120 mM glycine) at 110 V for 90 min. Blots were blocked overnight in 5%
510 skim milk in 10 mM Tris-HCl, 150 mM NaCl and 0.1% Tween-20 at pH 7.5 (TBST). Portions of
511 the blot were incubated with a primary antibodies for 2 h in 1% skim milk in TBST at room
512 temperature (RT). Antibodies used include: anti-candidalysin nanobody (1:5000), 6D11 anti-
513 SLO mAb (1:1000), CPTC-A1–3 anti-annexin A1 mAb (1:250), anti-annexin A2 mAb (1:1000),

514 anti-Alix mAb (1:250), MANLAC-4A7 anti-Lamin A/C mAb (1:250), AC-15 anti-β-actin mAb
515 (1:5000) or with rabbit polyclonal antibodies: anti-aerolysin, anti-annexin A6, anti-MEK, anti-
516 phospho-MEK [Ser217/Ser221], anti-ERK p44/42, anti-phospho-ERK[Thr202/Tyr404], each at
517 1:1000 dilution. Next, blots were washed 3x for 5 min in TBST and then incubated with HRP-
518 conjugated anti-mouse-IgG, anti-rabbit-IgG, or anti-alpaca V_{HH} antibodies (1:10,000) for 1 h in
519 1% skim milk in TBST at RT, washed 3x for 5 min in TBST, and developed with enhanced
520 chemiluminescence (ECL): either 0.01% H_2O_2 (Walmart, Fayetteville, AR, USA), 0.2 mM p-
521 Coumaric acid (Sigma), 1.25 mM Luminol (Sigma) in 0.1 M Tris-HCl pH 8.4, ECL Plus Western
522 Blotting Substrate (Cat# 32134), ECL Prime Western Blotting Reagent (Cat# RPN2232, Cytiva),
523 or Pierce ECL western blotting substrate (Cat#32106, ThermoFisher Scientific).

524 ***Statistics.*** Prism 10.4.1 (GraphPad, San Diego, CA, USA) or Excel were used for statistical
525 analysis. Data are represented as mean ± S.E.M. as indicated. The LC_{50} for toxins was
526 calculated by fitting % specific lysis curve to a logistic model in Excel as previously described[25].
527 Statistical significance was determined by regular or repeated measures one-way or two-way
528 ANOVA as described. $p<0.05$ was considered to be statistically significant. Graphs were
529 generated in Excel or Prism.

Acknowledgments

The authors would like to thank members of the Keyel lab for critical review of the manuscript. We thank colleagues for the generous gifts of reagents. We thank the College of Arts & Sciences Microscopy for use of facilities. This work was supported by American Heart Association grant 16SDG30200001, Texas Tech University, and NIH grant 1R21AI156225 to PAK. JRN was supported by grants from the Wellcome Trust (214229_Z_18_Z).

Author Contributions:

Conceptualization: RT, VK, BH, JRN, PAK

Methodology: RT, PAK

Investigation: RT, VK, PAK

Data Curation: RT, PAK

Formal Analysis: RT, PAK

Supervision: PAK

Resources: BH, JRN

Project Administration: PAK

Funding Acquisition: PAK

Writing—original draft: RT, VK, PAK

Writing—review & editing: RT, VK, BH, JRN, PAK

Conflicts of Interest: PAK is co-founder of Ardiyon Bio. The funders had no role in the design of the study; in the collection, analysis, or interpretation of data; in the writing of the manuscript; nor in the decision to publish the results.

Data and materials availability: All data are available in the main text or the supplementary materials.

556 **References**

557 1. Katsipoulaki, M., Stappers, M.H.T., Malavia-Jones, D., Brunke, S., Hube, B., and Gow,
558 N.A.R. (2024). Candida albicans and Candida glabrata: global priority pathogens.
559 Microbiology and molecular biology reviews : MMBR *88*, e0002123.
560 10.1128/mmbr.00021-23.
561 2. Schille, T.B., Sprague, J.L., Naglik, J.R., Brunke, S., and Hube, B. (2025).
562 Commensalism and pathogenesis of Candida albicans at the mucosal interface. Nat Rev
563 Microbiol. 10.1038/s41579-025-01174-x.
564 3. Moyes, D.L., Wilson, D., Richardson, J.P., Mogavero, S., Tang, S.X., Wernecke, J.,
565 Hofs, S., Gratacap, R.L., Robbins, J., Runglall, M., et al. (2016). Candidalysin is a fungal
566 peptide toxin critical for mucosal infection. Nature *532*, 64-68. 10.1038/nature17625.
567 4. Richardson, J.P., Brown, R., Kichik, N., Lee, S., Priest, E., Mogavero, S., Maufrais, C.,
568 Wickramasinghe, D.N., Tsavou, A., Kotowicz, N.K., et al. (2022). Candidalysins Are a
569 New Family of Cytolytic Fungal Peptide Toxins. mBio *13*, e0351021.
570 10.1128/mbio.03510-21.
571 5. Muller, R., Konig, A., Groth, S., Zarnowski, R., Visser, C., Handrianz, T., Maufrais, C.,
572 Kruger, T., Himmel, M., Lee, S., et al. (2024). Secretion of the fungal toxin candidalysin
573 is dependent on conserved precursor peptide sequences. Nature microbiology *9*, 669-
574 683. 10.1038/s41564-024-01606-z.
575 6. Russell, C.M., Schaefer, K.G., Dixson, A., Gray, A.L.H., Pyron, R.J., Alves, D.S., Moore,
576 N., Conley, E.A., Schuck, R.J., White, T.A., et al. (2022). The Candida albicans virulence
577 factor candidalysin polymerizes in solution to form membrane pores and damage
578 epithelial cells. eLife *11*. 10.7554/eLife.75490.
579 7. Lin, J., Miao, J., Schaefer, K.G., Russell, C.M., Pyron, R.J., Zhang, F., Phan, Q.T., Solis,
580 N.V., Liu, H., Tashiro, M., et al. (2024). Sulfated glycosaminoglycans are host epithelial
581 cell targets of the Candida albicans toxin candidalysin. Nature microbiology *9*, 2553-
582 2569. 10.1038/s41564-024-01794-8.
583 8. Zhang, T.Y., Chen, Y.Q., Tan, J.C., Zhou, J.A., Chen, W.N., Jiang, T., Zha, J.Y., Zeng,
584 X.K., Li, B.W., Wei, L.Q., et al. (2024). Global fungal-host interactome mapping identifies
585 host targets of candidalysin. Nat Commun *15*, 1757. 10.1038/s41467-024-46141-x.
586 9. Naglik, J.R., Gaffen, S.L., and Hube, B. (2019). Candidalysin: discovery and function in
587 Candida albicans infections. Curr Opin Microbiol *52*, 100-109.
588 10.1016/j.mib.2019.06.002.
589 10. Thapa, R., Ray, S., and Keyel, P.A. (2020). Interaction of Macrophages and Cholesterol-
590 Dependent Cytolysins: The Impact on Immune Response and Cellular Survival. Toxins
591 (Basel) *12*. 10.3390/toxins12090531.
592 11. Cooper, S.T., and McNeil, P.L. (2015). Membrane Repair: Mechanisms and
593 Pathophysiology. Physiol Rev *95*, 1205-1240. 10.1152/physrev.00037.2014.
594 12. Demonbreun, A.R., Quattrocelli, M., Barefield, D.Y., Allen, M.V., Swanson, K.E., and
595 McNally, E.M. (2016). An actin-dependent annexin complex mediates plasma membrane
596 repair in muscle. J Cell Biol *213*, 705-718. 10.1083/jcb.201512022.
597 13. Roostalu, U., and Strahle, U. (2012). In vivo imaging of molecular interactions at
598 damaged sarcolemma. Dev Cell *22*, 515-529. 10.1016/j.devcel.2011.12.008.
599 14. Lapaquette, P., Ducreux, A., Basmaciyan, L., Paradis, T., Bon, F., Bataille, A., Winckler,
600 P., Hube, B., d'Enfert, C., Esclatine, A., et al. (2022). Membrane protective role of
601 autophagic machinery during infection of epithelial cells by Candida albicans. Gut
602 Microbes *14*, 2004798. 10.1080/19490976.2021.2004798.
603 15. Keyel, P.A., Loultcheva, L., Roth, R., Salter, R.D., Watkins, S.C., Yokoyama, W.M., and
604 Heuser, J.E. (2011). Streptolysin O clearance through sequestration into blebs that bud
605 passively from the plasma membrane. J Cell Sci *124*, 2414-2423. jcs.076182 [pii]

606 10.1242/jcs.076182.
607 16. Ray, S., Roth, R., and Keyel, P.A. (2022). Membrane repair triggered by cholesterol-
608 dependent cytolysins is activated by mixed lineage kinases and MEK. Science advances
609 *8*, eabl6367. 10.1126/sciadv.abl6367.
610 17. Jimenez, A.J., Maiuri, P., Lafaurie-Janvore, J., Divoux, S., Piel, M., and Perez, F. (2014).
611 ESCRT machinery is required for plasma membrane repair. Science *343*, 1247136.
612 10.1126/science.1247136.
613 18. Romero, M., Keyel, M., Shi, G., Bhattacharjee, P., Roth, R., Heuser, J.E., and Keyel,
614 P.A. (2017). Intrinsic repair protects cells from pore-forming toxins by microvesicle
615 shedding. Cell Death Differ *24*, 798-808. 10.1038/cdd.2017.11.
616 19. Wolfmeier, H., Schoenauer, R., Atanassoff, A.P., Neill, D.R., Kadioglu, A., Draeger, A.,
617 and Babiychuk, E.B. (2015). Ca(2)(+)-dependent repair of pneumolysin pores: A new
618 paradigm for host cellular defense against bacterial pore-forming toxins. Biochim
619 Biophys Acta *1853*, 2045-2054. 10.1016/j.bbamcr.2014.09.005.
620 20. Thapa, R., and Keyel, P.A. (2023). Patch repair protects cells from the small pore-
621 forming toxin aerolysin. J Cell Sci *136*. 10.1242/jcs.261018.
622 21. Westman, J., Plumb, J., Licht, A., Yang, M., Allert, S., Naglik, J.R., Hube, B., Grinstein,
623 S., and Maxson, M.E. (2022). Calcium-dependent ESCRT recruitment and lysosome
624 exocytosis maintain epithelial integrity during Candida albicans invasion. Cell reports *38*,
625 110187. 10.1016/j.celrep.2021.110187.
626 22. Ho, J., Wickramasinghe, D.N., Nikou, S.A., Hube, B., Richardson, J.P., and Naglik, J.R.
627 (2020). Candidalysin Is a Potent Trigger of Alarmin and Antimicrobial Peptide Release in
628 Epithelial Cells. Cells *9*. 10.3390/cells9030699.
629 23. Sprague, J.L., Schille, T.B., Allert, S., Trumper, V., Lier, A., Grossmann, P., Priest, E.L.,
630 Tsavou, A., Panagiotou, G., Naglik, J.R., et al. (2024). Candida albicans translocation
631 through the intestinal epithelial barrier is promoted by fungal zinc acquisition and limited
632 by NFkappaB-mediated barrier protection. PLoS Pathog *20*, e1012031.
633 10.1371/journal.ppat.1012031.
634 24. Dal Peraro, M., and van der Goot, F.G. (2016). Pore-forming toxins: ancient, but never
635 really out of fashion. Nat Rev Microbiol *14*, 77-92. 10.1038/nrmicro.2015.3.
636 25. Haram, C.S., Moitra, S., Keane, R., Breslav, E., Zhang, K., and Keyel, P.A. (2022).
637 Deciphering the Molecular Mechanism and Function of Pore-Forming Toxins using
638 Leishmania major. J Vis Exp. 10.3791/64341.
639 26. Haram, C.S., Moitra, S., Keane, R., Kuhlmann, F.M., Frankfater, C., Hsu, F.F., Beverley,
640 S.M., Zhang, K., and Keyel, P.A. (2023). The sphingolipids ceramide and inositol
641 phosphorylceramide protect the Leishmania major membrane from sterol-specific toxins.
642 J Biol Chem *299*, 104745. 10.1016/j.jbc.2023.104745.
643 27. Schoenauer, R., Larpin, Y., Babiychuk, E.B., Drucker, P., Babiychuk, V.S., Avota, E.,
644 Schneider-Schaulies, S., Schumacher, F., Kleuser, B., Koffel, R., and Draeger, A.
645 (2019). Down-regulation of acid sphingomyelinase and neutral sphingomyelinase-2
646 inversely determines the cellular resistance to plasmalemmal injury by pore-forming
647 toxins. FASEB J *33*, 275-285. 10.1096/fj.201800033R.
648 28. Das, A., Brown, M.S., Anderson, D.D., Goldstein, J.L., and Radhakrishnan, A. (2014).
649 Three pools of plasma membrane cholesterol and their relation to cholesterol
650 homeostasis. eLife *3*, e02882. 10.7554/eLife.02882.
651 29. Skocaj, M., Resnik, N., Grundner, M., Ota, K., Rojko, N., Hodnik, V., Anderluh, G.,
652 Sobota, A., Macek, P., Veranic, P., and Sepcic, K. (2014). Tracking
653 cholesterol/sphingomyelin-rich membrane domains with the ostreolysin A-mCherry
654 protein. PLoS One *9*, e92783. 10.1371/journal.pone.0092783.

655 30. Endapally, S., Frias, D., Grzemska, M., Gay, A., Tomchick, D.R., and Radhakrishnan, A.
656 (2019). Molecular Discrimination between Two Conformations of Sphingomyelin in
657 Plasma Membranes. Cell. 10.1016/j.cell.2018.12.042.
658 31. Cabezas, S., Ho, S., Ros, U., Lanio, M.E., Alvarez, C., and van der Goot, F.G. (2017).
659 Damage of eukaryotic cells by the pore-forming toxin sticholysin II: Consequences of the
660 potassium efflux. Biochim Biophys Acta *1859*, 982-992. 10.1016/j.bbamem.2017.02.001.
661 32. Keyel, P.A., Roth, R., Yokoyama, W.M., Heuser, J.E., and Salter, R.D. (2013).
662 Reduction of streptolysin O (SLO) pore-forming activity enhances inflammasome
663 activation. Toxins (Basel) *5*, 1105-1118. 10.3390/toxins5061105.
664 33. Babiychuk, E.B., Monastyrskaya, K., Potez, S., and Draeger, A. (2011). Blebbing confers
665 resistance against cell lysis. Cell Death Differ *18*, 80-89. 10.1038/cdd.2010.81.
666 34. Bose, T., Cieslar-Pobuda, A., and Wiechec, E. (2015). Role of ion channels in regulating
667 Ca(2)(+) homeostasis during the interplay between immune and cancer cells. Cell death
668 & disease *6*, e1648. 10.1038/cddis.2015.23.
669 35. Ho, J., Yang, X., Nikou, S.A., Kichik, N., Donkin, A., Ponde, N.O., Richardson, J.P.,
670 Gratacap, R.L., Archambault, L.S., Zwirner, C.P., et al. (2019). Candidalysin activates
671 innate epithelial immune responses via epidermal growth factor receptor. Nat Commun
672 *10*, 2297. 10.1038/s41467-019-09915-2.
673 36. Stauber, T., and Jentsch, T.J. (2013). Chloride in vesicular trafficking and function. Annu
674 Rev Physiol *75*, 453-477. 10.1146/annurev-physiol-030212-183702.
675 37. Sun, R., Luo, Y., Li, J., Wang, Q., Li, J., Chen, X., Guan, K., and Yu, Z. (2015).
676 Ammonium chloride inhibits autophagy of hepatocellular carcinoma cells through
677 SMAD2 signaling. Tumour Biol *36*, 1173-1177. 10.1007/s13277-014-2699-x.
678 38. Namkung, W., Yao, Z., Finkbeiner, W.E., and Verkman, A.S. (2011). Small-molecule
679 activators of TMEM16A, a calcium-activated chloride channel, stimulate epithelial
680 chloride secretion and intestinal contraction. FASEB J *25*, 4048-4062. 10.1096/fj.11-
681 191627.
682 39. Wu, N., Cernysiov, V., Davidson, D., Song, H., Tang, J., Luo, S., Lu, Y., Qian, J.,
683 Gyurova, I.E., Waggoner, S.N., et al. (2020). Critical Role of Lipid Scramblase
684 TMEM16F in Phosphatidylserine Exposure and Repair of Plasma Membrane after Pore
685 Formation. Cell reports *30*, 1129-1140 e1125. 10.1016/j.celrep.2019.12.066.
686 40. Martins, J.R., Faria, D., Kongsuphol, P., Reisch, B., Schreiber, R., and Kunzelmann, K.
687 (2011). Anoctamin 6 is an essential component of the outwardly rectifying chloride
688 channel. Proc Natl Acad Sci U S A *108*, 18168-18172. 10.1073/pnas.1108094108.
689 41. Mogavero, S., Sauer, F.M., Brunke, S., Allert, S., Schulz, D., Wisgott, S., Jablonowski,
690 N., Elshafee, O., Kruger, T., Kniemeyer, O., et al. (2021). Candidalysin delivery to the
691 invasion pocket is critical for host epithelial damage induced by Candida albicans. Cell
692 Microbiol *23*, e13378. 10.1111/cmi.13378.
693 42. Tsitrin, Y., Morton, C.J., el-Bez, C., Paumard, P., Velluz, M.C., Adrian, M., Dubochet, J.,
694 Parker, M.W., Lanzavecchia, S., and van der Goot, F.G. (2002). Conversion of a
695 transmembrane to a water-soluble protein complex by a single point mutation. Nat Struct
696 Biol *9*, 729-733. 10.1038/nsb839.
697 43. Babiychuk, E.B., Monastyrskaya, K., Potez, S., and Draeger, A. (2009). Intracellular
698 Ca(2+) operates a switch between repair and lysis of streptolysin O-perforated cells. Cell
699 Death Differ *16*, 1126-1134.
700 44. Rescher, U., Zobiack, N., and Gerke, V. (2000). Intact Ca(2+)-binding sites are required
701 for targeting of annexin 1 to endosomal membranes in living HeLa cells. J Cell Sci *113 (*
702 *Pt 22)*, 3931-3938.
703 45. Skocaj, M., Bakrac, B., Krizaj, I., Macek, P., Anderluh, G., and Sepcic, K. (2013). The
704 sensing of membrane microdomains based on pore-forming toxins. Curr Med Chem *20*,
705 491-501.

706 46. Keyel, P.A., Heid, M.E., Watkins, S.C., and Salter, R.D. (2012). Visualization of bacterial
707 toxin induced responses using live cell fluorescence microscopy. J Vis Exp, e4227. 4227
708 [pii]

709 10.3791/4227.
710 47. Dany, M., and Ogretmen, B. (2015). Ceramide induced mitophagy and tumor
711 suppression. Biochim Biophys Acta *1853*, 2834-2845. 10.1016/j.bbamcr.2014.12.039.

712 **Figure Legends**

713 **Figure 1. Candidalysin killing is intermediate between aerolysin and CDCs.** HeLa cells
714 were challenged with (A) 9.375-600 HU/mL candidalysin (Clys), (B) 4-2000 HU/mL aerolysin
715 (Aero), (C) 31-2000 HU/mL SLO, or (A-C) a mass equivalent to wild-type toxin of
716 candidalysin^{mutAA}, aerolysin^{Y221G} , or monomer-locked SLO (SLO ML) in 2 mM $CaCl_2$
717 supplemented RPMI with 20 µg/ml propidium iodide (PI) at 37°C. PI uptake was analyzed by
718 flow cytometry and % specific lysis was determined. (D) The amount of toxin needed to kill 50%
719 of the cells (LC_{50}) was calculated by logistic modeling. (E) HeLa cells were challenged with
720 9.375-600 HU/mL Clys, 31-2000 HU/mL Aero, or 31-2000 HU/mL SLO at 37°C either in 2 mM
721 $CaCl_2$, or 2 mM EGTA supplemented RPMI. PI uptake was analyzed by flow cytometry. The
722 LC_{50} was calculated as described above. Dotted lines indicate the lower and upper limits of
723 detection. Graphs show the mean ± S.E.M. of (A-D) six or (E) five independent experiments,
724 with (D, E) independent experiments plotted as data points. * $p < 0.05$, ** $p<0.01$, *** $p<0.001$,
725 **** $p<0.0001$ by repeated-measures one-way ANOVA with Tukey's multiple comparison test.
726

727 **Figure 2. Patch repair and ceramide fail to protect cells against candidalysin.** (A) C2C12
728 cells stably expressing control (CTL) or *Dysf* shRNA were challenged with 9.375-600 HU/mL
729 candidalysin (Clys), 31-2000 HU/mL aerolysin (Aero), or 31-2000 HU/mL SLO. (B) HeLa cells
730 were untransfected or transfected with GFP or GFP-Dysferlin (GFP Dysf) for 48 h and then
731 challenged with 9.375-600 HU/mL Clys, 31-2000 HU/mL Aero, or 31-2000 HU/mL SLO. (C, D)
732 HeLa cells were pretreated with either vehicle DMSO (CTL) or 40 µM PPMP for 72 h. Cells were
733 then (C) challenged with 9.375-600 HU/mL Clys, 31-2000 HU/mL Aero, or 31-2000 HU/mL SLO
734 or (D) labeled with 20 µg/mL OlyA-mCherry WT or OlyA ^{E69A}-mCherry for 30 min. PI uptake or
735 OlyA-mCherry binding was analyzed by flow cytometry. The LC_{50} was calculated as described
736 in the methods. The dotted lines indicate the lower limits of detection (9.4 HU/mL for Clys, 31.25
737 HU/mL for Aero and SLO). Graphs show the mean ± S.E.M. of four independent experiments. *

738 p <0.05, ** p <0.01, **** p<0.0001, ns not significant by repeated-measures one-way ANOVA
739 with Tukey's multiple comparison test.
740
741 **Figure 3. Chloride ions protect cells from candidalysin.** (A) HeLa cells were challenged with
742 9.375-600 HU/mL candidalysin (Clys), 31-2000 HU/mL aerolysin (Aero), or 31-2000 HU/mL
743 SLO in RPMI supplemented with or without 150 mM KCl. (B) Caspase $1/11^{-/-}$ bone-marrow
744 derived macrophages (Casp$1/11^{-/-}$ MΦ) were challenged with Clys, Aero, or SLO in RPMI
745 supplemented with either 2 mM $CaCl_2$ or 2 mM EGTA, and/or 150 mM KCl. (C) HeLa cells were
746 challenged with Clys in RPMI supplemented 2 mM $CaCl_2$, 2 mM EGTA, 150 mM KCl and/or 20
747 μM nigericin alone or in combination. (D, E) HeLa cells were challenged with Clys, Aero, or SLO
748 in RPMI supplemented with 2 mM $CaCl_2$ and either: nothing, 150 mM NaCl, 150 mM KCl, 300
749 mM dextrose, 150 mM potassium acetate, or 150 mM NH_4Cl. PI uptake was analyzed by flow
750 cytometry. The dotted lines indicates the upper (600 HU/mL for Clys, 1000 HU/mL for Aero) and
751 lower limits (9.4 HU/mL for Clys, 125 HU/mL for SLO, 31 HU/mL or 0.5 HU/mL for Aero) of
752 detection. The LC_{50} was calculated as described in the methods. Graphs display independent
753 experiments and mean ± S.E.M. of (A, C, E) three or (B, D) four experiments. * p <0.05, **
754 p<0.01, *** p<0.001, ns not significant by (A, B, D, E) repeated-measures one-way ANOVA with
755 Tukey's multiple comparison test or (C) repeated-measures two-way ANOVA with Geisser-
756 Greenhouse correction and Šídák's multiple comparisons test.
757
758 **Figure 4. MEK activation provides limited protection against candidalysin.** HeLa cells were
759 serum starved for 30 min and pre-treated with 20 μM MEK inhibitor U0126 or DMSO for 30 min.
760 (A) Cells were then challenged with sublytic toxin concentrations (50 HU/mL Clys, 62 HU/mL
761 aerolysin Aero or 250 HU/mL SLO) and analyzed by western blot. Blots were probed with the
762 indicated antibodies and HRP-conjugated secondary antibodies. (B-D) Serum starved and
763 DMSO or U0126-treated Hela cells were challenged with (B) 9.375-600 HU/mL Clys, (C) 31-

764 2000 HU/mL Aero, or (D) 31-2000 HU/mL SLO either in 2 mM $CaCl_2$ or 2 mM EGTA
765 supplemented RPMI. PI uptake was analyzed by flow cytometry. The LC_{50} was calculated as
766 described in the methods. The dotted lines indicate the upper and lower limits of detection. One
767 representative blot from three independent experiments is shown. Graphs show four
768 independent experiments, and the mean ± S.E.M. ** $p<0.01$, *** $p<0.001$, **** $p<0.0001$ by
769 repeated-measures one-way ANOVA with Tukey's multiple comparison test compared to DMSO
770 Ca^{2+}.
771
772 **Figure 5. Annexins provide limited protection against candidalysin.** (A-C) HeLa cells were
773 transfected with control (CTL), annexin A1 (A1), annexin A2 (A2) or annexin A6 (A6) siRNA for
774 3 days and then (A, B) lysed for western blot analysis, or (C) challenged with 9.375-600 HU/mL
775 candidalysin (Clys), 31-2000 HU/mL aerolysin (Aero), or 31-2000 HU/mL SLO. PI uptake was
776 analyzed by flow cytometry. The LC_{50} was calculated as described in the methods. (A) Portions
777 of the blot were probed with antibodies against A1, A2, A6 or β-actin followed by HRP-
778 conjugated secondary antibodies. (B) Blots were quantified by densitometry and the knockdown
779 efficiency compared to control siRNA determined. (D-F) A2-GFP or (G-I) A6-YFP transfected
780 HeLa cells were challenged with sublytic toxin concentrations (50 HU/mL Clys, 62 HU/mL Aero,
781 or 250 HU/mL SLO) or a mass equivalent of mutant candidalysin ($Clys^{mutAA}$). Cells were imaged
782 by confocal microscopy for ~45 min at 37°C and then lysed using 1% Triton-X-100. The (D, G)
783 fraction of cells showing annexin membrane translocation is shown. For cells showing annexin
784 translocation, the time to half maximal ($t_{1/2}$) (E, H) cytosolic depletion or (F, I) membrane
785 accumulation of A2 or A6 is shown. The dotted lines indicate the upper and lower limits of
786 detection. The blots show one representative experiment from three independent experiments.
787 Graphs show the mean ± S.E.M. Individual data points represent (B) each of three independent
788 experiments or (E, F, H, I) individual cells from 3 independent experiments. * $p<0.05$, ** $p<0.01$,

789 *** $p<0.00$, **** $p<0.0001$ by (C, D, G) repeated measures or (E, F, H, I) regular one-way
790 ANOVA with Tukey's multiple comparison test.
791
792 **Figure 6. Candidalysin is removed via membrane shedding.** HeLa cells were challenged
793 with sublytic toxin concentrations (50 HU/mL candidalysin (Clys), 62 HU/mL aerolysin (Aero) or
794 250 HU/mL SLO) or a mass equivalent of mutant candidalysin ($Clys^{mutAA}$). Cells were
795 centrifuged at 2000xg for 5 min to yield cell pellets (denoted C). Cell supernatants were spun at
796 100,000xg for 40 min at 4°C for the microvesicle pellet (MV). Proteins were resolved by SDS-
797 PAGE and analyzed by western blot using the indicated primary antibodies. The blots show one
798 representative experiment from four independent experiments.
799
800 **Figure 7. Candidalysin is resisted by distinct repair mechanisms compared to bacterial**
801 **PFTs.** After pore formation and membrane damage by each toxin, multiple repair pathways are
802 triggered downstream of Ca^{2+} flux. Candidalysin induces a protective Cl^- influx and activates
803 MEK-dependent repair, which contributes to cell protection. Annexin translocation occurs slowly
804 and provides minor protection, while patch repair is ineffective. In contrast, aerolysin does not
805 benefit from Cl^- influx or MEK protection. Aerolysin triggers moderate annexin translocation and
806 relies primarily on patch repair as the main protective mechanism. Streptolysin O elicits rapid
807 annexin translocation and activates MEK signaling, both of which contribute to robust protection.
808 Patch repair plays only a minor protective role against SLO. The figure was created using
809 BioRender.

810 **Supplemental Tables**

811 **Supplementary Table S1. Lytic parameters of toxins used**

Toxin	Figure Used	Hemolytic Activity (HU/mL)	Protein Concentration (mg/mL)	Specific Activity (HU/mg)
Candidalysin WT	1A, D, E, 2A-C, 3A-E, 4A, B, 5C-I, 6A, S1A, S2A, S3A-D, S4A-E, S5A, S6A, S7A-C	5×10^4	10	5×10^3
Candidalysin^{mutAA}	1A, 5D, G, 6A, S7A-C	5×10^3	10	5×10^2
Aerolysin WT	1B, D, 2A, B, 3A, 4A, C, 5C, D-I, 6A, S3B, C, S4A, S5B, S6B, S7A-C	4×10^5	2.8	1.43×10^5
	1E, 2C, 3B-E, 7A, S1B, S2B, S3A, D, S4B-E,	6.7×10^5	2.4	2.8×10^5
Aerolysin^{Y221G}	1B	$<1 \times 10^3$	1.6	$<6.25 \times 10^2$
SLO WT	1C-E, 3A, S1C, S2C, S3A, S4A	6×10^5	1.5	4×10^5
	2B, 3B, C, 4D, 5C-I, 6A, S3B, S4B, C, S5C, S6C, S7A-C	1×10^6	2.4	4.2×10^5
	2A, C, D, 3B-E, 4A, 5C, S3B, D, S4B-E, S6C	2×10^6	5.3	3.8×10^5
SLO ML	1C	$<1 \times 10^3$	3.2	$<3.13 \times 10^2$

812

813

814 **Supplemental Figure Legends**

815 **Supplementary Figure S1. Cytolytic activity of Candidalysin increases at 1 h.** HeLa cells
816 were challenged with (A) candidalysin (Clys), (B) aerolysin (Aero) or (C) streptolysin O (SLO) at
817 the indicated concentrations in 2 mM $CaCl_2$ supplemented, phenol-red free DMEM for 30 min, 1
818 h and 2 h. Viability of cells was assessed by MTT assay and % specific lysis was determined.
819 The LC_{50} was calculated as described in the methods. Graphs display mean ± S.E.M of 3
820 independent experiments, with individual points representing independent experiments. The
821 dotted lines indicate the limits of detection. * $p < 0.05$, ns not significant by repeated-measures
822 ANOVA with Tukey post-test.

823

824 **Supplementary Figure S2. LDH assay under-reports killing by toxins.** HeLa cells were
825 challenged with (A) candidalysin (Clys), (B) aerolysin (Aero) and (C) SLO at the indicated
826 concentrations in 2 mM $CaCl_2$ supplemented, phenol-red free DMEM for 30 min, 1 h and 2 h.
827 Cells were centrifuged at 1200xg for 5 min and cell pellet and supernatant were separated. The
828 % specific lysis and raw cytotoxicity was determined by LDH assay. The graphs display the
829 mean ± S.E.M of 3 independent experiments. * $p < 0.05$, ** $p < 0.01$ by repeated-measures
830 ANOVA with Tukey post-test.
831
832 **Supplementary Figure S3. Ca^{2+} dependent repair is essential for cellular protection**
833 **against candidalysin but not patch repair and ceramide.** (A) HeLa cells or (B) C2C12 control
834 and *Dysf* shRNA cells were challenged with the indicated concentrations of candidalysin (Clys),
835 aerolysin (Aero) or SLO in RPMI with 20 µg/ml PI supplemented with either 2 mM $CaCl_2$ or (A) 2
836 mM EGTA. (C) HeLa cells were either untransfected, or transfected with GFP or GFP Dysferlin
837 (GFP-Dysf) for 48 h and challenged with 9.375-600 HU/mL of Clys, or 31-2000 HU/mL of Aero
838 for 1 h or challenged with the indicated concentrations of Clys, Aero or SLO. (D) HeLa cells
839 were pretreated with either DMSO (CTL) or 40 µM PPMP for 72 h. Then cells were challenged
840 with the indicated concentrations of Clys, Aero or SLO. PI uptake was analyzed by flow
841 cytometry and specific lysis was determined. Graphs show the mean ± S.E.M of (A) 5 or (B-D) 4
842 independent experiments.
843
844 **Supplementary Figure S4. Chloride ions play a crucial role in protecting cells from**
845 **candidalysin.** (A) HeLa cells were challenged with the indicated concentrations of candidalysin
846 (Clys), aerolysin (Aero), or SLO in RPMI supplemented with or without 150 mM KCl. (B)
847 Caspase $1/11^{-/-}$ bone-marrow derived macrophages were challenged with the indicated
848 concentrations of Clys, Aero or SLO in RPMI supplemented with 2 mM $CaCl_2$ or 2 mM EGTA
849 and/or 150 mM KCl. (C) HeLa cells were challenged with Clys at indicated concentrations in

850 RPMI supplemented with the indicated combinations of 2 mM $CaCl_2$, 2 mM EGTA, 20 μM
851 nigericin or 150 mM KCl. (D, E) HeLa cells were challenged with the indicated concentrations of
852 Clys, Aero or SLO in RPMI with 2 mM $CaCl_2$ supplemented nothing (Ca^{2+}), 300 mM dextrose,
853 150 mM NaCl, 150 mM KCl, 150 mM potassium acetate, or 150 mM NH_4Cl. PI uptake was
854 analyzed by flow cytometry and specific lysis was determined. Graphs show the mean ± S.E.M.
855 of (A, C, E) 3 or (B, D) 4 independent experiments.
856
857 **Supplementary Figure S5. Calcium-mediated MEK activation promotes limited cellular**
858 **resistance to candidalysin.** HeLa cells were serum starved for 30 min and pre-treated with 20
859 μM MEK inhibitor U0126 or vehicle DMSO for 30 min. Cells were challenged either in 2 mM
860 $CaCl_2$ or 2 mM EGTA supplemented RPMI with the indicated concentrations of (A) candidalysin
861 (Clys), (B) aerolysin (Aero), or (C) SLO. PI uptake was analyzed by flow cytometry and specific
862 lysis was determined. Graphs show the mean ± S.E.M of 4 independent experiments.
863
864 **Supplementary Figure S6. Transient deletion of annexins sensitizes cells to candidalysin.**
865 HeLa cells were transfected with siRNAs to control (CTL) or annexins for 72 h. Cells were then
866 challenged with indicated concentrations of (A) candidalysin (Clys), (B) aerolysin (Aero), or (C)
867 SLO. PI uptake was analyzed by flow cytometry and specific lysis was determined. Graphs
868 show the mean ± SEM of (A-C) 3 independent experiments.
869
870 **Supplementary Figure S7. Delayed translocation of annexins occurs following**
871 **candidalysin challenge.** HeLa cells transfected with A2-GFP or A6-YFP were challenged with
872 sublytic toxin concentrations (50 HU/mL candidalysin (Clys), 62 HU/mL aerolysin (Aero) or 250
873 HU/mL SLO) or a mass equivalent of mutant candidalysin ($Clys^{mutAA}$). The cells were imaged by
874 confocal microscopy for ~45 min at 37°C and then lysed with 1% Triton-X-100. The mean ±
875 SEM of (A) annexin depletion from the cytosol, (B) annexin enrichment on the membrane, or (C)

876 TO-PRO3 uptake over time is graphed normalized to maximal intensity. For each toxin, 25–30
877 cells from 3 independent experiments were analyzed. Arrowheads indicate toxin addition or
878 Triton addition.
879
880 **Supplementary Figure S8. Original Western blots for Fig 4.** Uncropped blots from Fig 5 are
881 shown.
882
883 **Supplementary Figure S9. Original Western blots for Fig 5.** Uncropped blots from Fig 5 are
884 shown.
885
886 **Supplementary Figure S10. Original Western blots for Fig 6.** Uncropped blots from Fig 5 are
887 shown.
888
889 **Supplemental Video Legends**
890 **Video V1. Cells utilize annexin A6 mediated microvesicle shedding to remove**
891 **candidalysin pores.** HeLa cells transfected with annexin A6-YFP (green) were challenged with
892 sublytic (A) candidalysin (CLY WT), (B) mutant candidalysin (CLY mutAA), (C) aerolysin (Aero),
893 or (D) SLO in the presence of 2 μg/mL TO-PRO3 (blue) and imaged at 37°C by live cell
894 confocal imaging at 1-3.5 frame/second. Triton-X-100 was added at the end of 45 min of
895 imaging as a positive control for cell permeabilization. Images were bleach-corrected by
896 histogram matching. Time shows min after toxin addition. Scale bar = 10 μm.
897
898 **Video V2. Candidalysin triggers delayed annexin A2 translocation to membrane.** HeLa
899 cells transfected with annexin A2-GFP (green) were challenged with sublytic (A) candidalysin
900 (CLY WT), (B) mutant candidalysin (CLY mutAA), (C) aerolysin (Aero), or (D) SLO in the
901 presence of 2 μg/mL TO-PRO3 (blue) and imaged at 37°C by live cell confocal imaging at 1-3.5

902 frame/second. Triton-X-100 was added at the end of 45 min of imaging as a positive control for
903 cell permeabilization. Images were bleach-corrected by histogram matching. Time shows min
904 after toxin addition. Scale bar = 10 μm.

Figure 1

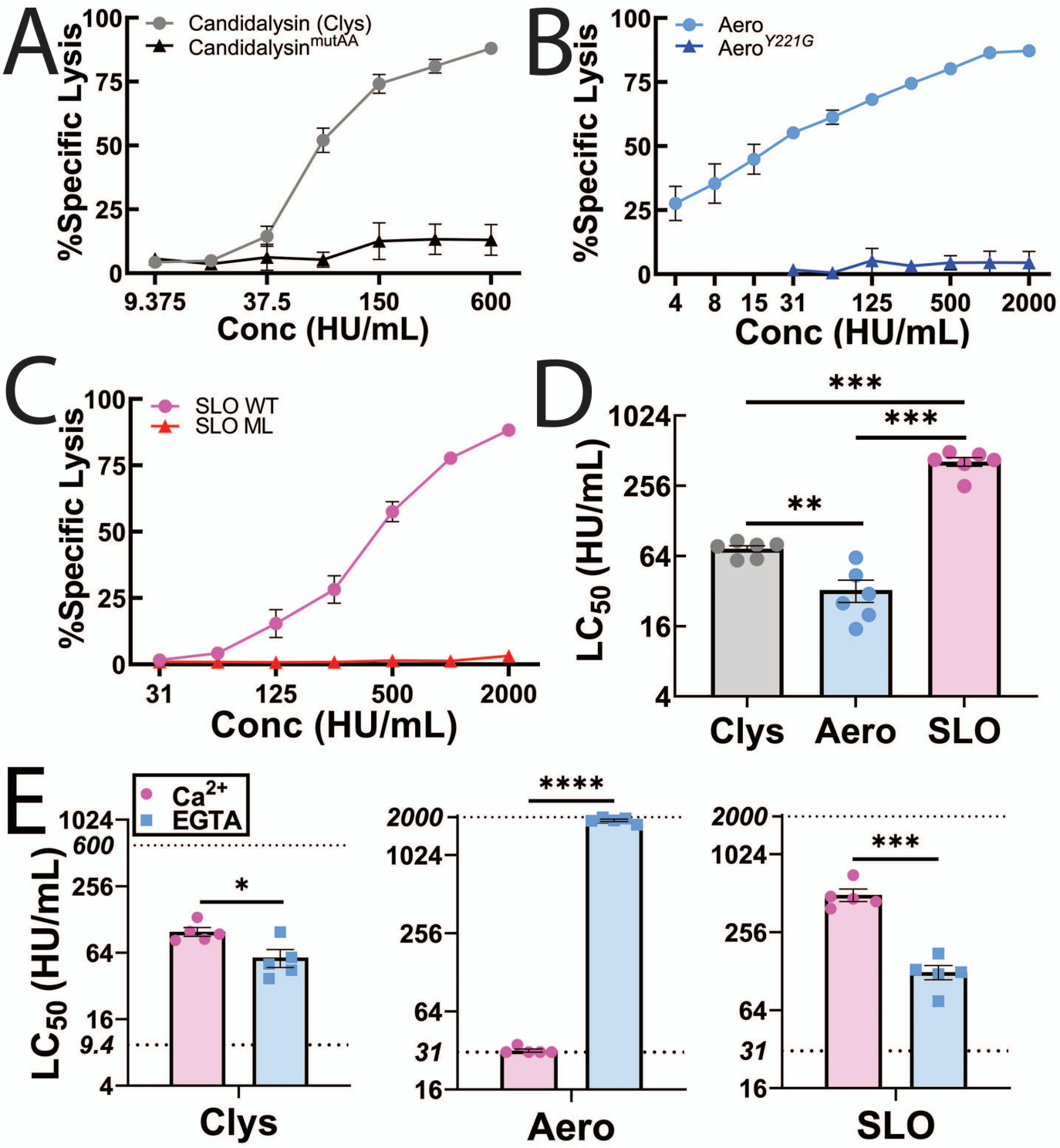
A
Candidalysin (Clys)
Candidalysin^{mutAA}
%Specific Lysis
100
75
50
25
0
9.375
37.5
150
600
Conc (HU/mL)
B
Aero
Aero^{Y221G}
%Specific Lysis
100
75
50
25
0
4
8
15
31
125
500
2000
Conc (HU/mL)
C
SLO WT
SLO ML
%Specific Lysis
100
75
50
25
0
31
125
500
2000
Conc (HU/mL)
D
***
***
**
LC_{50} (HU/mL)
1024
256
64
16
4
Clys
Aero
SLO
E
Ca^{2+}
EGTA
LC_{50} (HU/mL)
1024
600
256
64
16
9.4
4
*
Clys
****
2000
1024
256
64
31
16
Aero
2000
1024
256
64
31
16
***
SLO

Figure 2

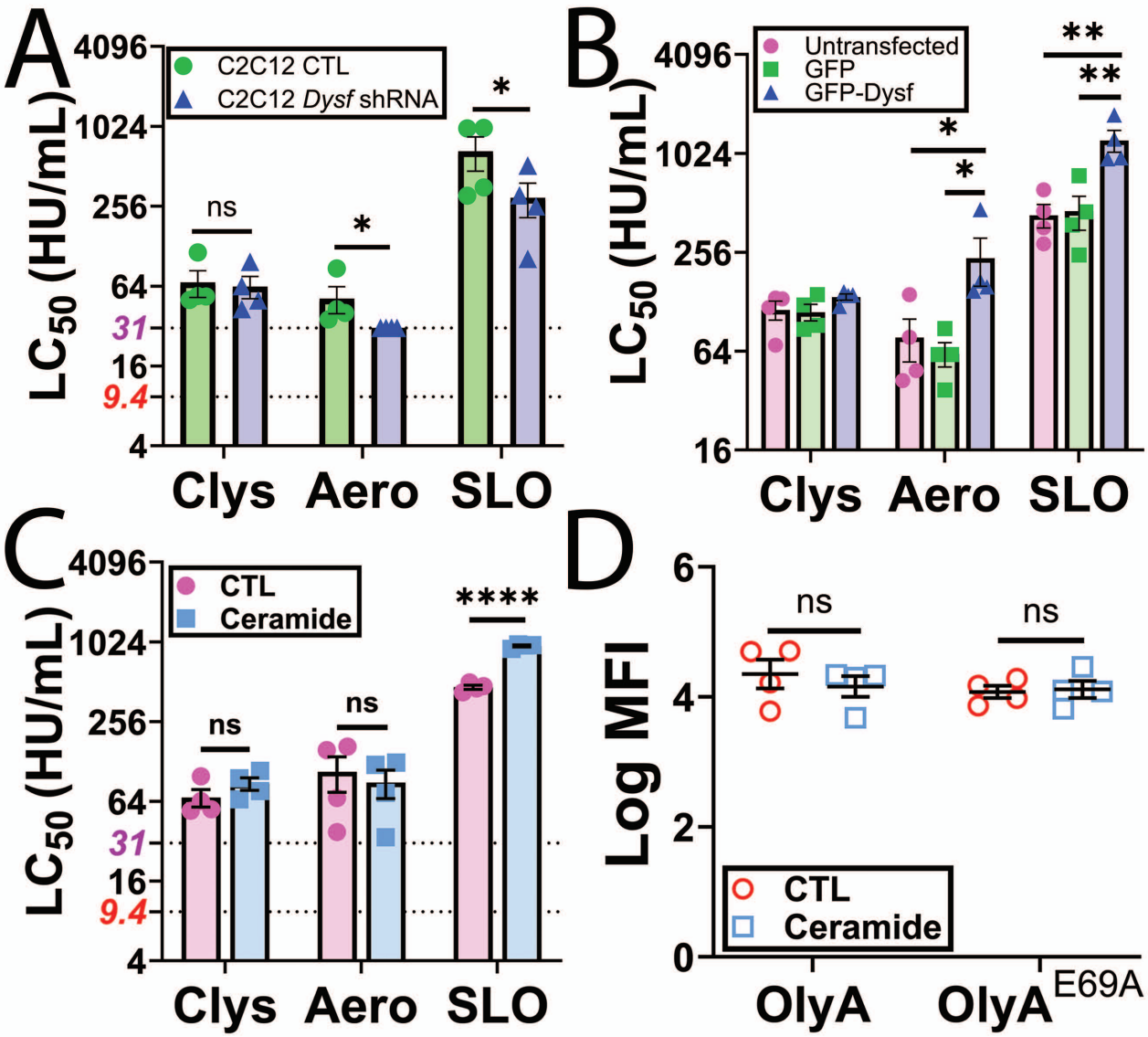
A
C2C12 CTL
C2C12 Dysf shRNA
LC50 (HU/mL)
4096
1024
256
64
31
16
9.4
4
ns
*
*
Clys
Aero
SLO
B
Untransfected
GFP
GFP-Dysf
LC50 (HU/mL)
4096
1024
256
64
16
*
*
**
**
Clys
Aero
SLO
C
CTL
Ceramide
LC50 (HU/mL)
4096
1024
256
64
31
16
9.4
4
ns
ns
****
Clys
Aero
SLO
D
Log MFI
6
4
2
0
ns
ns
CTL
Ceramide
OlyA
OlyA E69A

Figure 3

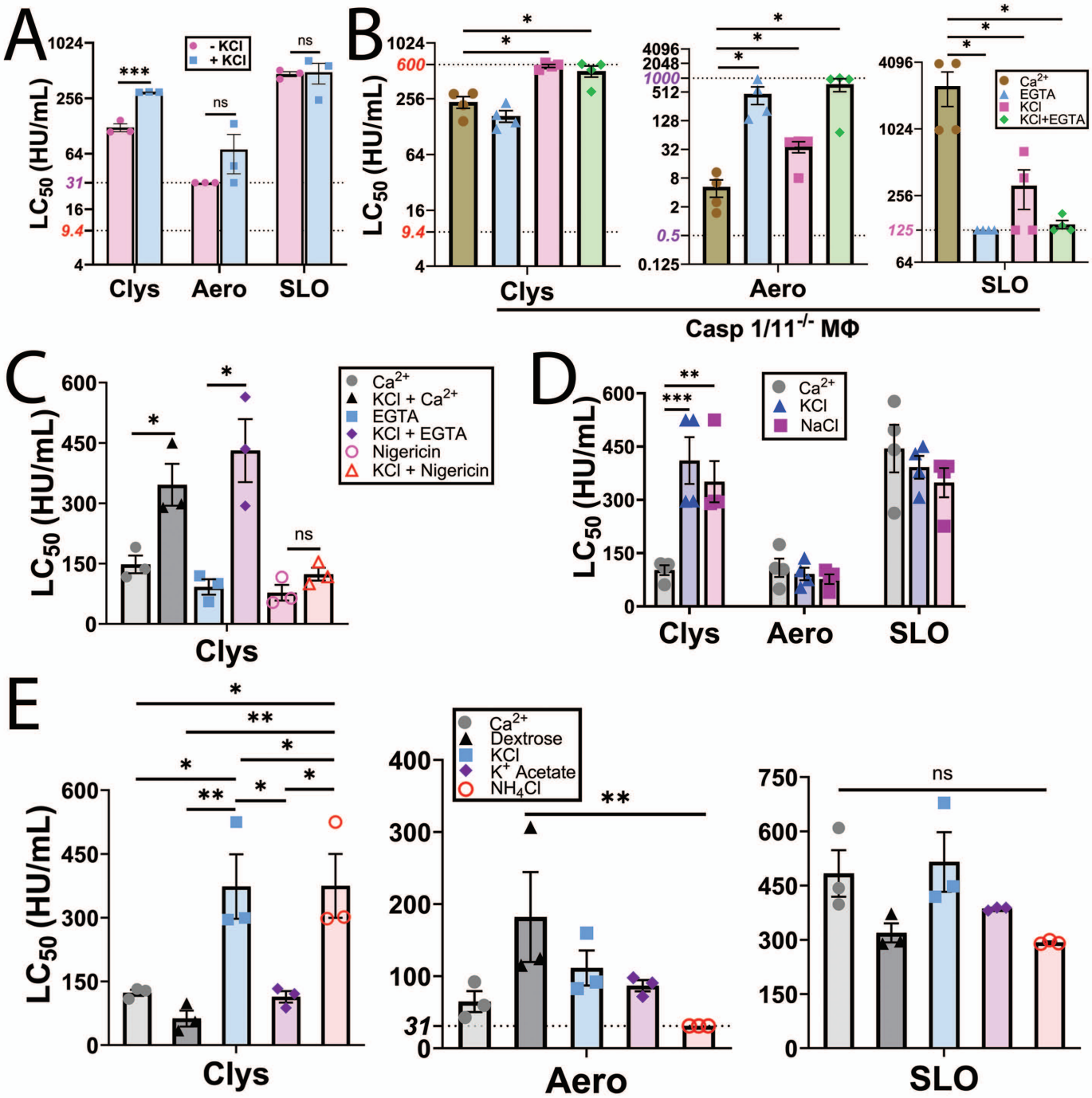
A
- KCl
+ KCl
LC50 (HU/mL)
1024
256
64
31
16
9.4
4
***
ns
ns
Clys
Aero
SLO
B
600
1000
0.5
125
Ca2+
EGTA
KCl
KCl+EGTA
Casp 1/11-/- MΦ
C
Ca2+
KCl + Ca2+
EGTA
KCl + EGTA
Nigericin
KCl + Nigericin
D
Ca2+
KCl
NaCl
E
Ca2+
Dextrose
KCl
K+ Acetate
NH4Cl

Figure 4

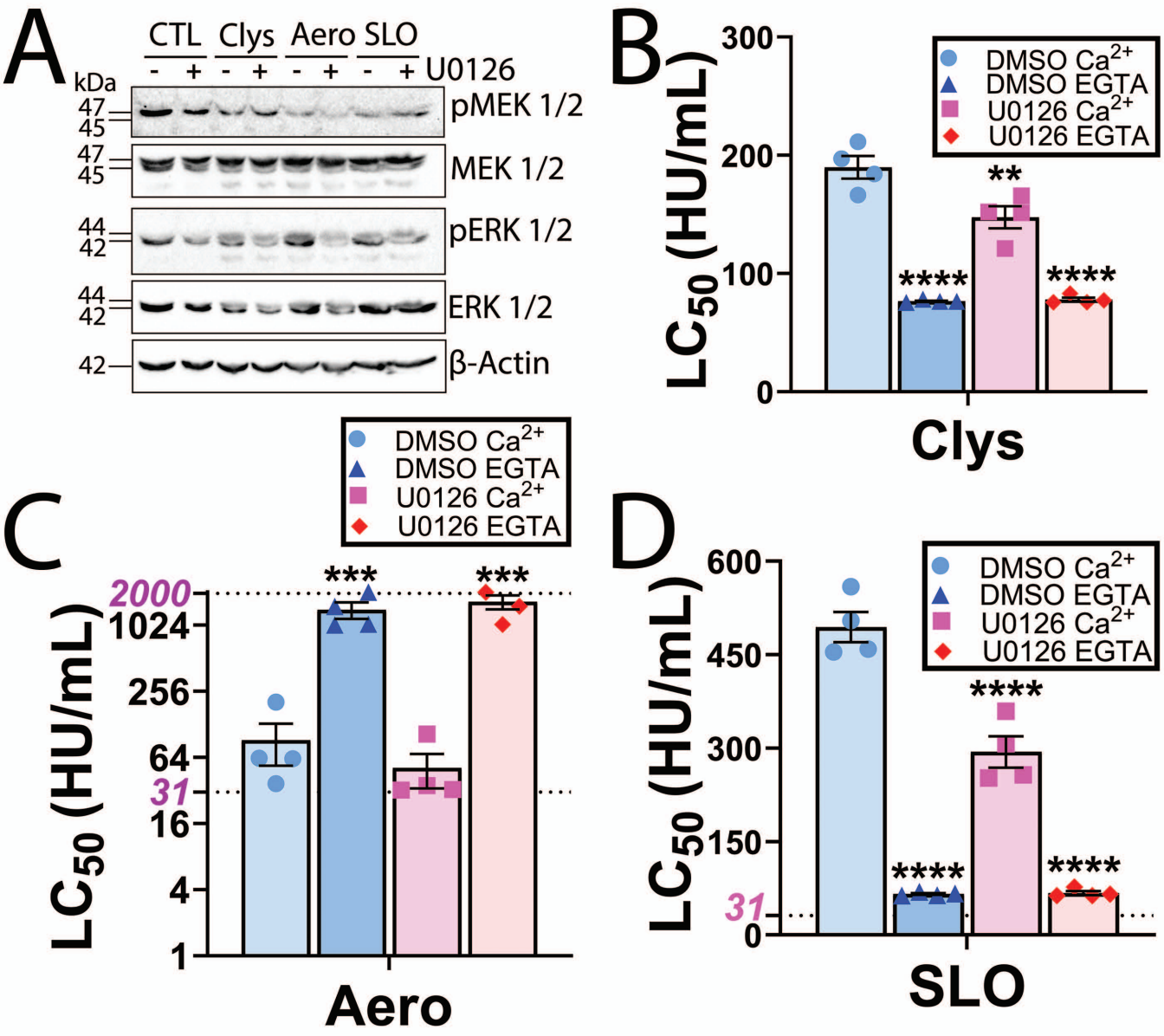
A
CTL
Clys
Aero
SLO
U0126
kDa
47
45
pMEK 1/2
MEK 1/2
44
42
pERK 1/2
ERK 1/2
β-Actin
B
DMSO Ca2+
DMSO EGTA
U0126 Ca2+
U0126 EGTA
LC50 (HU/mL)
Clys
C
Aero
D
SLO

Figure 5

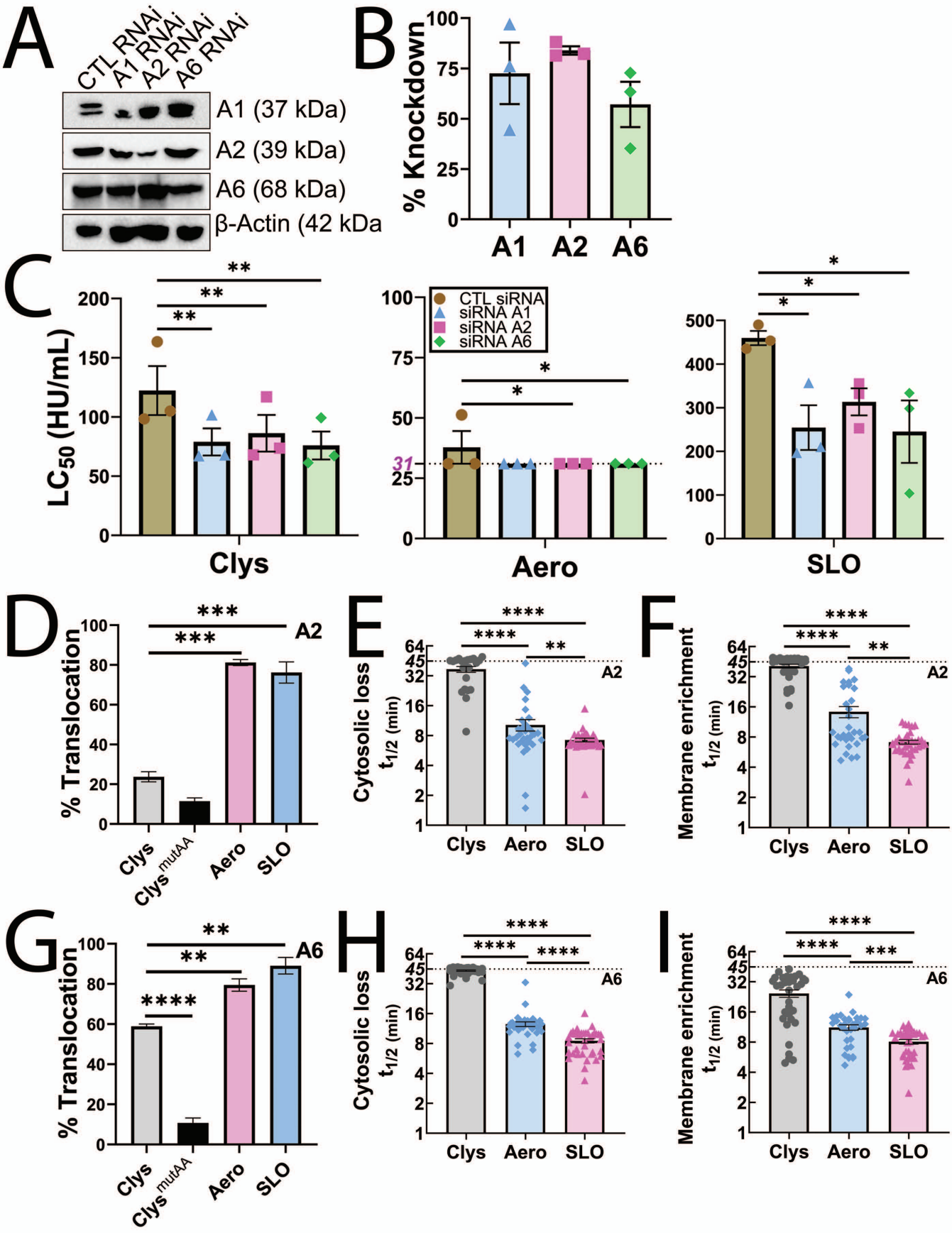
A
CTL RNAi
A1 RNAi
A2 RNAi
A6 RNAi
A1 (37 kDa)
A2 (39 kDa)
A6 (68 kDa)
β-Actin (42 kDa
B
% Knockdown
A1
A2
A6
C
LC50 (HU/mL)
CTL siRNA
siRNA A1
siRNA A2
siRNA A6
Clys
Aero
SLO
D
% Translocation
A2
Clys
Clys mutAA
Aero
SLO
E
Cytosolic loss
t1/2 (min)
A2
F
Membrane enrichment
t1/2 (min)
A2
G
% Translocation
A6
H
Cytosolic loss
t1/2 (min)
A6
I
Membrane enrichment
t1/2 (min)
A6

Figure 6

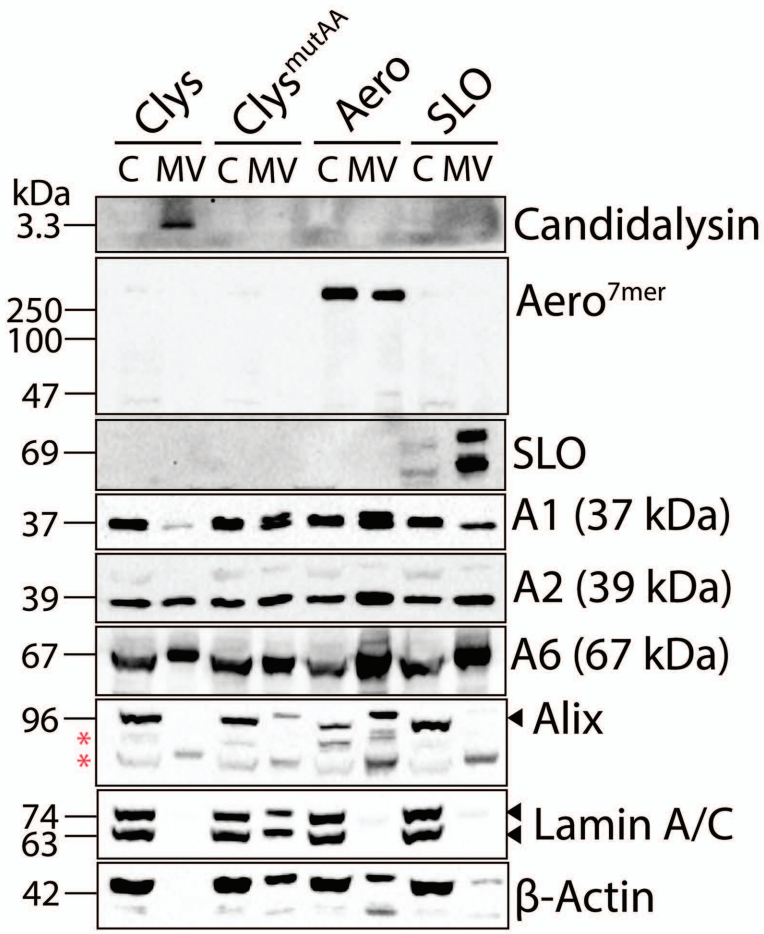
Clys
Clys^mutAA
Aero
SLO
C MV C MV C MV C MV
kDa
3.3
Candidalysin
250
100
47
Aero^7mer
69
SLO
37
A1 (37 kDa)
39
A2 (39 kDa)
67
A6 (67 kDa)
96
Alix
74
63
Lamin A/C
42
β-Actin

Figure 7

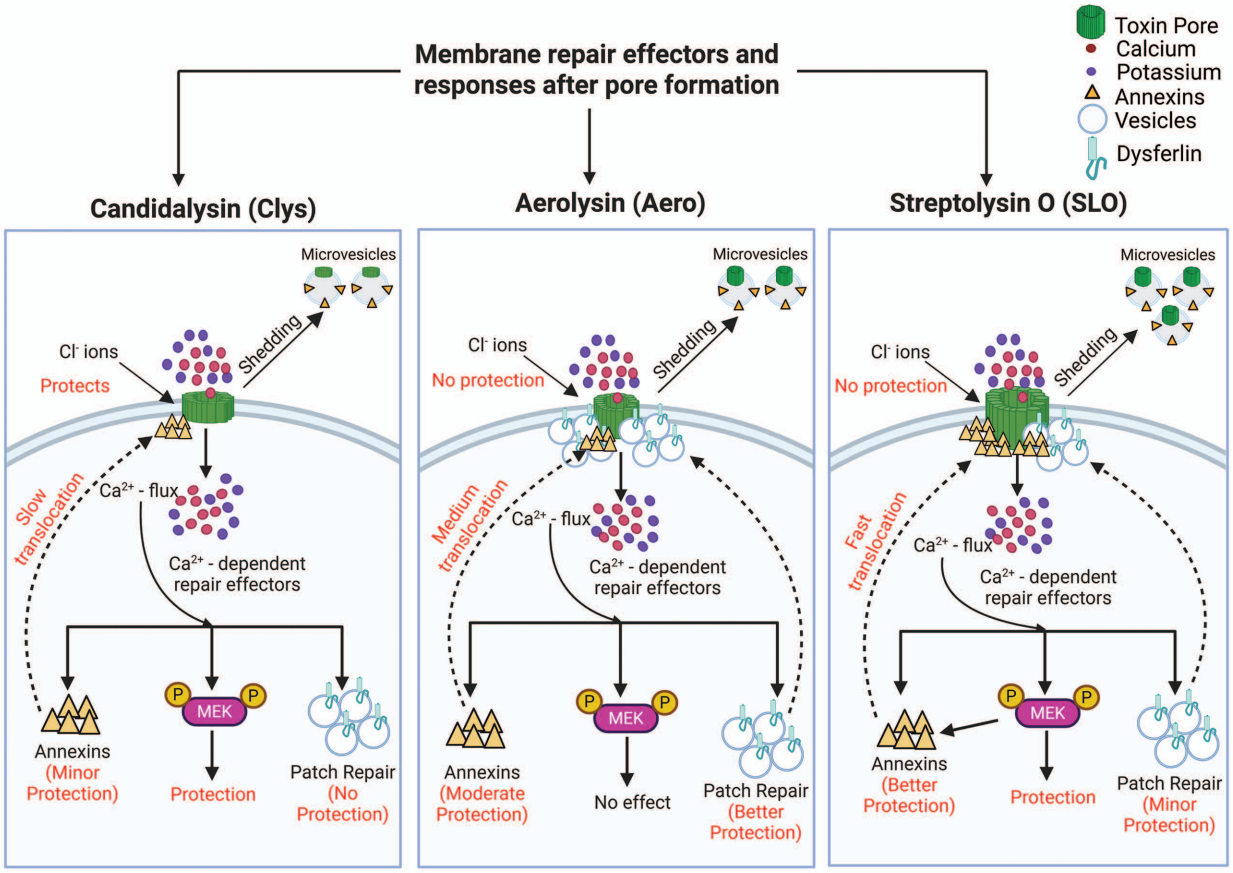
Membrane repair effectors and responses after pore formation
Toxin Pore
Calcium
Potassium
Annexins
Vesicles
Dysferlin
Candidalysin (Clys)
Aerolysin (Aero)
Streptolysin O (SLO)
Microvesicles
Shedding
Cl⁻ ions
Protects
No protection
No protection
Slow translocation
Medium translocation
Fast translocation
Ca²⁺ - flux
Ca²⁺ - dependent repair effectors
P
MEK
Annexins (Minor Protection)
Protection
Patch Repair (No Protection)
Annexins (Moderate Protection)
No effect
Patch Repair (Better Protection)
Annexins (Better Protection)
Protection
Patch Repair (Minor Protection)